



**HAL**  
open science

## Precipitation frequency in Med-CORDEX and EURO-CORDEX ensembles from 0.44° to convection-permitting resolution: impact of model resolution and convection representation

Minh Ha, Sophie Bastin, Philippe Drobinski, Lluís Fita, Jan Polcher, Olivier Bock, Marjolaine Chiriaco, Danijel Belušić, Cécile Caillaud, A. Dobler, et al.

### ► To cite this version:

Minh Ha, Sophie Bastin, Philippe Drobinski, Lluís Fita, Jan Polcher, et al.. Precipitation frequency in Med-CORDEX and EURO-CORDEX ensembles from 0.44° to convection-permitting resolution: impact of model resolution and convection representation. *Climate Dynamics*, 2024, 62, pp.4515-4540. 10.1007/s00382-022-06594-6 . insu-03916220v2

**HAL Id: insu-03916220**

**<https://insu.hal.science/insu-03916220v2>**

Submitted on 23 Sep 2024

**HAL** is a multi-disciplinary open access archive for the deposit and dissemination of scientific research documents, whether they are published or not. The documents may come from teaching and research institutions in France or abroad, or from public or private research centers.

L'archive ouverte pluridisciplinaire **HAL**, est destinée au dépôt et à la diffusion de documents scientifiques de niveau recherche, publiés ou non, émanant des établissements d'enseignement et de recherche français ou étrangers, des laboratoires publics ou privés.



Distributed under a Creative Commons Attribution 4.0 International License



# Precipitation frequency in Med-CORDEX and EURO-CORDEX ensembles from 0.44° to convection-permitting resolution: impact of model resolution and convection representation

Minh T. Ha<sup>1</sup> · Sophie Bastin<sup>1</sup> · Philippe Drobinski<sup>2</sup> · L. Fita<sup>3</sup> · J. Polcher<sup>2</sup> · O. Bock<sup>4,5</sup> · M. Chiriaco<sup>1</sup> · D. Belušić<sup>6,17</sup> · C. Caillaud<sup>7</sup> · A. Dobler<sup>8</sup> · J. Fernandez<sup>9</sup> · K. Goergen<sup>10</sup> · Ø. Hodnebrog<sup>11</sup> · S. Kartsios<sup>12</sup> · E. Katragkou<sup>12</sup> · A. Lavin-Gullon<sup>9</sup> · T. Lorenz<sup>13</sup> · J. Milovac<sup>9</sup> · H.-J. Panitz<sup>14</sup> · S. Sobolowski<sup>13</sup> · H. Truhetz<sup>15</sup> · K. Warrach-Sagi<sup>16</sup> · V. Wulfmeyer<sup>16</sup>

Received: 28 February 2022 / Accepted: 11 November 2022 / Published online: 29 December 2022  
© The Author(s) 2022

## Abstract

Recent studies using convection-permitting (CP) climate simulations have demonstrated a step-change in the representation of heavy rainfall and rainfall characteristics (frequency-intensity) compared to coarser resolution Global and Regional climate models. The goal of this study is to better understand what explains the weaker frequency of precipitation in the CP ensemble by assessing the triggering process of precipitation in the different ensembles of regional climate simulations available over Europe. We focus on the statistical relationship between tropospheric temperature, humidity and precipitation to understand how the frequency of precipitation over Europe and the Mediterranean is impacted by model resolution and the representation of convection (parameterized vs. explicit). We employ a multi-model data-set with three different resolutions (0.44°, 0.11° and 0.0275°) produced in the context of the MED-CORDEX, EURO-CORDEX and the CORDEX Flagship Pilot Study "Convective Phenomena over Europe and the Mediterranean" (FPSCONV). The multi-variate approach is applied to all model ensembles, and to several surface stations where the integrated water vapor (IWV) is derived from Global Positioning System (GPS) measurements. The results show that all model ensembles capture the temperature dependence of the critical value of IWV (IWV<sub>cv</sub>), above which an increase in precipitation frequency occurs, but the differences between the models in terms of the value of IWV<sub>cv</sub>, and the probability of its being exceeded, can be large at higher temperatures. The lower frequency of precipitation in convection-permitting simulations is not only explained by higher temperatures but also by a higher IWV<sub>cv</sub> necessary to trigger precipitation at similar temperatures, and a lower probability to exceed this critical value. The spread between models in simulating IWV<sub>cv</sub> and the probability of exceeding IWV<sub>cv</sub> is reduced over land in the ensemble of models with explicit convection, especially at high temperatures, when the convective fraction of total precipitation becomes more important and the influence of the representation of entrainment in models thus becomes more important. Over lowlands, both model resolution and convection representation affect precipitation triggering while over mountainous areas, resolution has the highest impact due to orography-induced triggering processes. Over the sea, since lifting is produced by large-scale convergence, the probability to exceed IWV<sub>cv</sub> does not depend on temperature, and the model resolution does not have a clear impact on the results.

**Keywords** Precipitation triggering · Convection-permitting models · Convection processes · Integrated water vapor

## 1 Introduction

Regional climate models (RCMs) are developed to provide regional details by downscaling General Circulation Models (GCMs) output. With fine-scale information for regional features, RCMs can give some added value compared to GCMs (Giorgi 2019). RCMs can describe more realistic near-surface wind speed over complex coastal areas (Winterfeldt and

✉ Minh T. Ha  
minh.ha@latmos.ipsl.fr

Extended author information available on the last page of the article

Weisse 2009), improve describing mesoscale variability of near-surface pressure and temperature (Feser and von Storch 2005), they are also able to capture well the average statistics of daily moderate precipitation on scales of a few grid boxes (Boberg et al. 2008; Kjellström et al. 2010). Despite refinements in resolution (12–50 km) and efforts to revise the dynamical and physical processes in RCMs, rainfall extremes are still poorly represented by the models even at regional scales (IPCC report AR6, 2021). Models tend to overestimate weak precipitation (Bastin et al. 2019; Stephens et al. 2010) and underestimate heavy rainfall (Lenderink and van Meijgaard 2008).

In GCMs and RCMs, deep convection, which is a dominant source of summer precipitation, is represented by using convection parameterization schemes. However, the inherent assumptions made in such schemes have been identified as a major source of errors and uncertainties in climate models (Hohenegger et al. 2008; Foley 2010; Kendon et al. 2012; Ban et al. 2014). For example, RCMs with parameterized convection can produce a too early onset of daytime moist convection in the warm season (Brockhaus et al. 2008), which affects convective potential energy and leads to a simulation of too frequent light precipitation (Dai and Trenberth 2004). Additionally, the poor representation of the interaction between subgrid-scale soil moisture and atmospheric temperature anomalies (Froidevaux et al. 2014) can exhibit a positive soil moisture-precipitation feedback and amplify perturbations of the hydrological cycle (Hohenegger et al. 2009). Recently, with the advances in high-performance computing, convection-permitting models (CPMs) with horizontal grid spacing less than ~4 km, which are traditionally used in weather forecasting, have begun to be applied on climate-time scales (Hohenegger et al. 2008; Kendon et al. 2017; Prein et al. 2015). At these resolutions, the parameterization of deep convection is not required (Prein et al. 2015; Weisman et al. 1997), providing hope that model uncertainties and parameter sensitivity may be reduced.

Several long-term simulations have been conducted with CPMs in the last decade over different areas, mainly Europe and the USA (e.g. Ban et al. 2014, 2021; Kendon et al. 2012, 2014; Rasmussen et al. 2011, 2014; Rasmussen et al. 2020; Keller et al. 2016; Prein et al. 2015; Leutwyler et al. 2017; Liu et al. 2017; Berthou et al. 2020; Hodnebrog et al. 2019; Fumière et al. 2020; Knist et al. 2020) and a few over other areas (e.g. Kouadio et al. 2020; Berthou et al. 2019; Kendon et al. 2019; Guo et al. 2019, 2020; Ahrens et al. 2020; Konduru and Takahashi 2020; Argüeso et al. 2020). These studies emphasize the added value of CPMs in representing precipitation over orographic regions, focusing more specifically on convective organization, the diurnal cycle of convection precipitation, the spatial structure of rainfall and its duration-intensity characteristics, and the intensity of hourly precipitation

extremes (see Lucas-Picher et al. 2021 for a review). However, the frequency of precipitation, which tends to be overestimated in RCMs at coarser resolution, seems to be underestimated in summer compared to available observational datasets (Ban et al. 2021). Even if these studies show promising improvements, only a few of them identify the processes underlying such improvements (e.g. Rasmussen et al. 2020). Convection triggering processes in particular are not well investigated despite the fact that they have a strong impact on the entire precipitation distribution and more specifically on extreme precipitation.

Properly representing convection is critical to successful simulations and ensuing water resources assessments. Convection can be viewed conceptually as being driven by the buoyancy realized by parcels being lifted to their level of free convection and rising freely into the local environment. Yet, it can be argued that moisture is a key component for convection, since convective parameterization is simply a method to account for the effects of subgrid-scale saturation. From this perspective, the moisture content drives the behavior of the convective scheme, controlling the amount of convection produced in an unstable environment based upon the available moisture that can be removed from the atmosphere. Convective parameterizations attempt to represent the dependence of the statistics of moist convection on water vapor and temperature. This forms the basis of many convective parameterizations and a better knowledge of this relationship in climate models would help to improve precipitation simulation. Therefore, we analyze the triggering of precipitation based on the relationship between precipitation, integrated water vapor (IWV) and tropospheric temperature. IWV has been identified as a better proxy than saturation vapor pressure for precipitation triggering in the Tropics (Neelin et al. 2009; Sahany et al. 2012). Over Europe this relationship was found to be consistent with studies conducted in the Tropics (Bastin et al. 2019). Comparisons of observations and some simulations in the HYMEX/Med-CORDEX programs showed deviations of IWV between models with parameterized deep convection over Europe at high temperature, giving some insights in the way this relationship could help in the investigation of model's spread. By using the tropospheric temperature instead of surface temperature, and the integrated water vapor instead of surface humidity, it allows to take into account the lower tropospheric environment which strongly conditions deep convection. In addition, the objective of this study is to test this relationship "temperature, IWV and precipitation" whatever the regime of precipitation and for all seasons including transitional seasons (fall and spring), to see how this relationship can help to understand the biases linked to parameterization of deep convection or low resolution. So the idea is to not discriminate atmospheric situations, nor seasons to test how

much the use of IWV and tropospheric temperature include the effects of different atmospheric circulations and stability.

In this study, we investigate the impact of model resolution and convection representation on the triggering of precipitation over Europe and the Mediterranean area. Model ensembles with three different resolutions (0.44°, 0.11° and 0.0275°) are used. At 0.0275°, deep convection is explicitly represented while at 0.44 and 0.11°, it is parameterized with different deep convection schemes. Simulations were performed in the frame of the EURO- (Jacob et al. 2014) and Med-CORDEX (Ruti et al. 2016) projects, and of their shared Flagship Pilot Study (FPS) on “Convective phenomena at high resolution over Europe and the Mediterranean” (Coppola et al. 2020; Ban et al. 2021).

The structure of the paper is as follows: Sect. 2 presents the data and methodology of this study. Section 3 presents results on the analysis of the impact of the model resolution and convection representation on precipitation triggering, and Sect. 4 assesses the discrepancy between the different ensembles. Finally, Sect. 5 provides a summary and conclusion.

## 2 Data and methods

### 2.1 Model simulations

As mentioned in the introduction, we have collected those simulations from Med-CORDEX, EURO-CORDEX and FPS on convection (FPSCONV), which provide the variables

required in our methodology (Sect. 2.3). The high resolution convection-permitting simulations (2.2 to 3 km) use explicit deep convection and cover the greater Alpine region (Fig. 1) for the period 2000–2009. These simulations are generally embedded in an outer domain covering the EURO-CORDEX area at 12 or 15 km grid spacing. This provides pairs of simulations suitable for the assessment of the effects of convection representation and resolution. Therefore, the analysis will be done over the FPSCONV domain, which is a common area of the Med-CORDEX, EURO-CORDEX and FPSCONV experiments, to assess: (1) the role of increased resolution and (2) the role of explicit convection over the period 2001–2008, which is the common period of the three ensembles. Additionally, three subareas (black boxes in Fig. 1) are chosen to analyze in more detail the model performance in different terrain including: (1) high orography over the mountains of the Alps (5–13°E, 45.5–47°E), (2) the Mediterranean Sea (4–8°E, 40.8–42.5°E) and (3) continental plains (2–12°E, 47.5–49°E).

The ensemble at 0.44° grid spacing (hereafter EUR-44) includes 4 simulations of the Med-CORDEX project and 6 simulations of the EURO-CORDEX project (Table 1). For the simulations at 0.11° grid spacing (EUR-11) ensemble, we have collected 3 simulations of the EURO-CORDEX project and the 9 remaining members are the simulations that drive the convection-permitting models over the Alpine region (Table 2). This sub-ensemble of 9 simulations is named ALP-11 and will give fair comparisons with high resolution (0.0275°) convection-permitting simulations (ALP-3). Six simulations are using version 3.8.1 of

**Fig. 1** Evaluation domain with the GPS locations (red dots) and SIRTAs (blue dot) used for comparison with simulations. Topography elevation (with a horizontal resolution of 3 km) is shown in color (units in m). The three black boxes indicate subareas (mountains of the Alps, the Mediterranean Sea, and plains) analyzed in more detail in the study

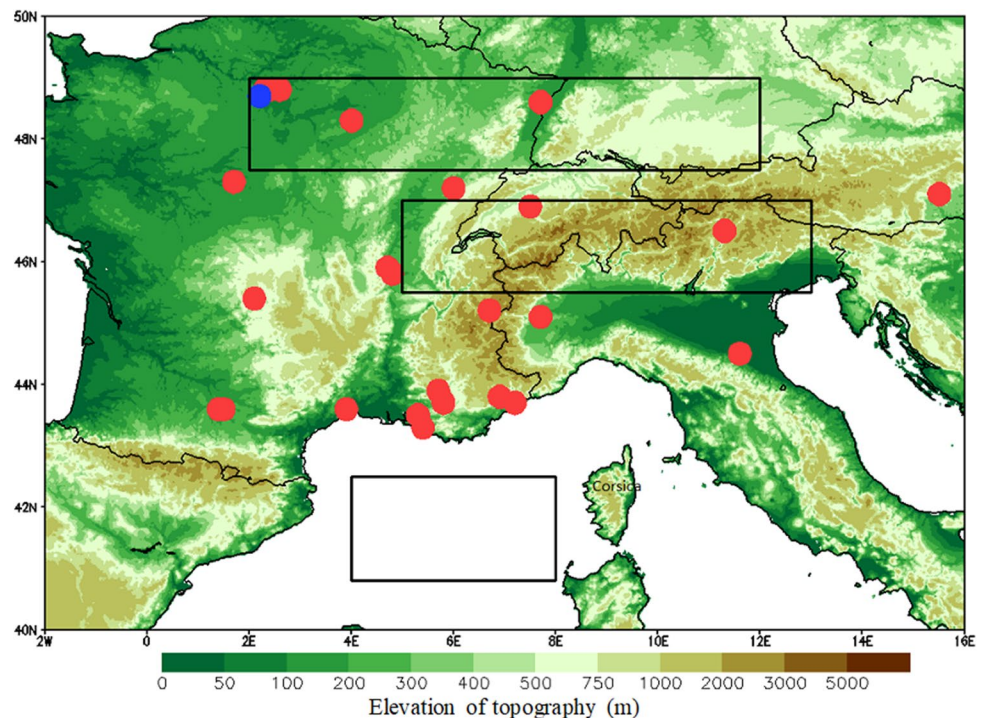


**Table 1** List of ERA-Interim driven simulations at 0.44° used in this study (referred to as EUR-44)

Group abbreviation	Group Full name	Model	Domain
IPSL	Institut Pierre-Simon-Laplace (France)	WRF311	MED-CORDEX
UCLM	Universidad de Castilla-La Mancha (Spain)	UCLM	MED-CORDEX
CNRM	Centre National de Recherches Meteorologiques (France)	ALADIN52	MED-CORDEX
CMCC	Centro Euro-Mediterraneo sui Cambiamenti Climatici (Italy)	CCLM4-8-19	MED-CORDEX
DMI	Danish Meteorological Institute (Denmark)	HIRHAM5	EURO-CORDEX
HMS	Hungarian Meteorological Service (Hungary)	ALADIN52	EURO-CORDEX
KNMI	Royal Netherlands Meteorological Institute (Netherlands)	RACMO22E	EURO-CORDEX
MOHC	Met Office Hadley Centre (England)	HadRM3P	EURO-CORDEX
SMHI	Swedish Meteorological and Hydrological Institute (Sweden)	RCA4	EURO-CORDEX
UCAN	Universidad de Cantabria (Spain)	WRF341I	EURO-CORDEX

**Table 2** List of ERA-Interim driven simulations at 0.11° and 0.0275° used in this study. The twelve 0.11° simulations are referred to as EUR-11 ensemble and the last nine simulations as ALP-11 (ALP-11 is a sub-ensemble of EUR-11). The 0.0275° simulations are referred to as ALP-3. Please note the FPSCONV WRF RCMs' ALP-3 domain is driven by a 15 km European domain run, covering the same area as the EUR-11 EURO-CORDEX domain

Group abbreviation	Group Full name	Model and grid spacing [km] used over EUR /Med CORDEX domain	Model and nested grid spacing [km] used over Alpine domain
DMI	Danish Meteorological Institute (Denmark)	HIRHAM5 / 12	
KNMI	Royal Netherlands Meteorological Institute (Netherlands)	RACMO22E / 12	
SMHI	Swedish Meteorological and Hydrological Institute (Sweden)	RCA4 / 12	
HCLIMcom	HARMONIE-Climate community Danish Meteorological Institute and MET Norway and Swedish Meteorological and Hydrological Institute (Sweden)	HCLIM38-ALADIN / 12	HCLIM38-AROME / 3
AUTH	Aristotle University of Thessaloniki (Greece)	WRF381BG / 15	WRF381BG / 3
CICERO	Center for International Climate Research (Norway)	WRF381BJ / 15	WRF381BJ / 3
CNRM	Centre National de Recherches Meteorologiques (France)	CNRM-ALADIN62 / 12 (using spectral nudging)	CNRM-AROME41t1. / 2.5
FZJ	Research Centre Juelich (Germany)	WRF381BB / 15	WRF381BB / 3
UCAN	Universidad de Cantabria (Spain)	WRF381BI / 15	WRF381BI / 3
UHOH	University of Hohenheim (Germany)	WRF381BD / 15	WRF381BD / 3
WEGC	Wegener Center for Climate and Global Change, Univ. of Graz (Austria)	WRF381BL / 15	WRF381BL / 3
KIT	Karlsruhe Institute of Technology (Germany)	COSMO-CLM / 25	COSMO-CLM / 3

the WRF model (Skamarock et al. 2008) with the same configuration and initial and boundary forcings. Only physics schemes differ between them (the last letter indicates a different physics configuration; Lavin-Gullon et al. (2021) gives more details on this multi-physics ensemble). One simulation is using CNRM-ALADIN62 (Nabat et al. 2020), one HCLIM38-ALADIN (Belušić et al. 2020), and the last one is using COSMO-CLM (Rockel et al. 2008;

Baldauf et al. 2011). Precipitation from all these simulations have been evaluated in Ban et al. (2021).

The ALP-3 ensemble (9 simulations) has a higher resolution and a different representation of deep convection that is explicitly resolved. Two ALP-3 models have some other differences in physical parameterizations compared to their parent configurations and hence different names, as described in the corresponding references: CNRM-AROME41t1

(Caillaud et al. 2021) and HCLIM38-AROME (Belušić et al. 2020). In order to provide a comparison at the same resolution with their driving simulations, we remapped the outputs of ALP-3 to the EUR-11 grid (ALP-3remapEUR-11) using conservative remapping.

## 2.2 Reference data

To compare model results with observations, we used available gridded precipitation products (for an estimate of daily precipitation occurrence), and stations where we can get IWV, tropospheric temperature, and precipitation rate.

For IWV, we selected 25 Global Positioning System (GPS) stations (Table 3) distributed throughout the domain (red dots in Fig. 1) and for which the available data coverage is at least 4 years of the evaluation period (2001–2008). The GPS dataset used in this study is based on homogeneously reprocessed GPS delay data produced by IGN. It contains 6-hourly, daily and monthly Zenith Tropospheric Delay (ZTD) and IWV estimates for more than 400 stations over France and Europe. The original ZTD data were screened

and converted into IWV using surface pressure and weighted mean temperatures computed from ERA5 pressure-level data. The daily values were computed as weighted averages of 00, 06, 12, 18 UTC of the day and 00UTC of the next day. More information on the processing and post-processing procedures and options can be found in Bock (2021), including a link to download the data.

To complement these GPS stations, this study also uses observations collected since 2003 at the SIRTAs atmospheric observatory (blue dot on Fig. 1), located 20-km South West of Paris (Haeffelin et al. 2005). This observatory has collected many observations, which are now synthesized into the so-called “SIRTA-ReOBS” dataset described in Chiriaco et al. (2018) and used in Chiriaco et al. (2014) and Bastin et al. (2018, 2019). GPS IWV and precipitation rates are available in this dataset, and the advantage of this type of station is the collocation of the measurements of all variables. For tropospheric temperature, we used the radio soundings launched twice a day a few kilometers from SIRTAs.

For the other stations, tropospheric temperature is extracted from the European Centre for Medium-Range

**Table 3** List of GPS stations used in this study

Stations	Province/Country	Latitude	Longitude	Altitude (m)	Period	Number of non-missing values
AXPV	Aix-En-Provence/France	43.49121475	5.33319521	179.526398	2002–2008	1504
BSCN	Besancon/France	47.24687958	5.98938465	310.606384	2001–2008	1884
BZRG	Bolzano/Italy	46.49902344	11.3367958	279.552094	2001–2008	1391
EGLT	Egletons/France	45.40335083	2.05199409	616.033936	2001–2008	1916
GINA	France	43.67572403	5.78697968	331.485809	2001–2008	1911
GRAS	Caussols/France	43.75473785	6.92057228	1269.36096	2001–2008	2222
GRAZ	Graz/Austria	47.06713104	15.4934788	490.8508	2001–2008	2349
MARS	Marseille/France	43.27877045	5.35378599	12.4186001	2001–2008	2225
MDOR	Saint-Didier-au-Mont-d'Or/France	45.79901886	4.80895758	280.781586	2002–2008	1801
MEDI	Medicina/Italy	44.5199585	11.6468134	9.64779949	2001–2008	2250
MICH	France	43.92415619	5.71735287	577.435791	2001–2008	1929
MLVL	Marne-la-Vallee/France	48.84105682	2.58730984	115.980797	2001–2008	2075
MODA	France	45.21377563	6.71008444	1129.13391	2001–2008	1649
MTPL	France	43.63743591	3.86483932	69.8919983	2001–2008	1741
NICA	France	43.70326233	7.22726059	207.646393	2002–2008	1492
OPMT	Paris/France	48.83591843	2.33493781	78.0371018	2002–2008	1849
SJDV	Saint-Jean-des-Vignes/France	45.87908554	4.67657423	382.418915	2001–2008	1689
SMNE	Saint-Mande/France	48.84444427	2.42502046	81.7205963	2001–2008	2333
STJ9	France	48.62166214	7.68381643	188.723404	2001–2008	2010
TLMF	Toulouse/France	43.57460785	1.37509692	171.992599	2002–2008	1618
TLSE	Toulouse/France	43.56069565	1.48088932	158.102707	2001–2008	2227
TORI	Torino/Italy	45.06336594	7.66128016	262.679779	2001–2008	2157
TRYS	France	48.29424667	4.01181555	122.274399	2002–2008	1807
VFCH	Villefranche-sur-Cher/France	47.29419327	1.71967316	106.545097	2001–2008	1866
ZIMM	Zimmerwald/Switzerland	46.87709808	7.46527576	907.471191	2001–2008	2405

Weather Forecasts (ECMWF) reanalysis ERA5 (Hersbach et al. 2019). ERA5 is the fifth generation of the ECMWF atmospheric reanalysis that has been operational at ECMWF since 2016. This new reanalysis replaces the ERA-Interim reanalysis and covers the period from 1950 until the present (currently, the period 1950–1978 is only preliminary released). ERA5 is based on the Integrated Forecasting System (IFS) Cy41r2 which was the operational weather forecasting model in 2016, combined with the best available observational data from satellites and in situ stations around the world into a globally complete and consistent dataset.

For precipitation, we used different national gridded products of daily precipitation with a resolution below 8 km:

- EURO4M-APGD is available at a horizontal resolution of 5 km over the Alpine region from 1971–2008. This dataset is based on daily rain gauge station data and is presented in Isotta et al (2014).
- SAFRAN: The SAFRAN meteorological analysis is a mesoscale atmospheric analysis system for surface variables. It provides meteorological data over France on a 8 km grid at the hourly time step using observed data and atmospheric simulations. Further details on the SAFRAN analysis system can be found in Quintana-Seguí et al. (2008) and Vidal et al. (2010).
- REGNIE (Regionalisierte Niederschlagshöhen) is a gridded dataset of daily precipitation with 1 km horizontal resolution provided by the hydrometeorologic department of Deutscher Wetterdienst. It covers Germany and is a multiple regression interpolation product based on

geography and inverse distance weighting (Rauthe et al. 2013).

### 2.3 Method to analyze precipitation triggering based on the relationship between IWV and precipitation as a function of temperature

The method to establish the relationship between IWV and precipitation as a function of tropospheric temperature was introduced in detail in Bastin et al. (2019). Here we introduced some modifications to the method in order to adapt it to the new observational datasets used in this study and for the comparison between models at different resolutions. The analysis period is 2001–2008, when the maximum number of simulations and observations are available, with the exception of the SIRTA station, which covers the period 2008–2015. Using a different period can slightly affect the results, but SIRTA is still of interest because it is collocated with other measurements. An assessment of the impact of the selected period has been done in Bastin et al. (2019) and shows the match for the overlapping period. We therefore decided to keep this station so that we can have a reference from observations to compare with model outputs in the continental plains analysis subarea.

Tropospheric temperature is calculated as the average of the 2 m temperature and the 850, 500, and 200 hPa temperature as in Bastin et al. (2019) but, here, we split the tropospheric temperature into 1 K size bins instead of 4 K to discover some changes in the behavior of the model that may occur in only a small temperature range (Fig. 2). For each temperature bin, the daily total precipitation (mm/day) are sorted by increasing values of daily mean IWV, then

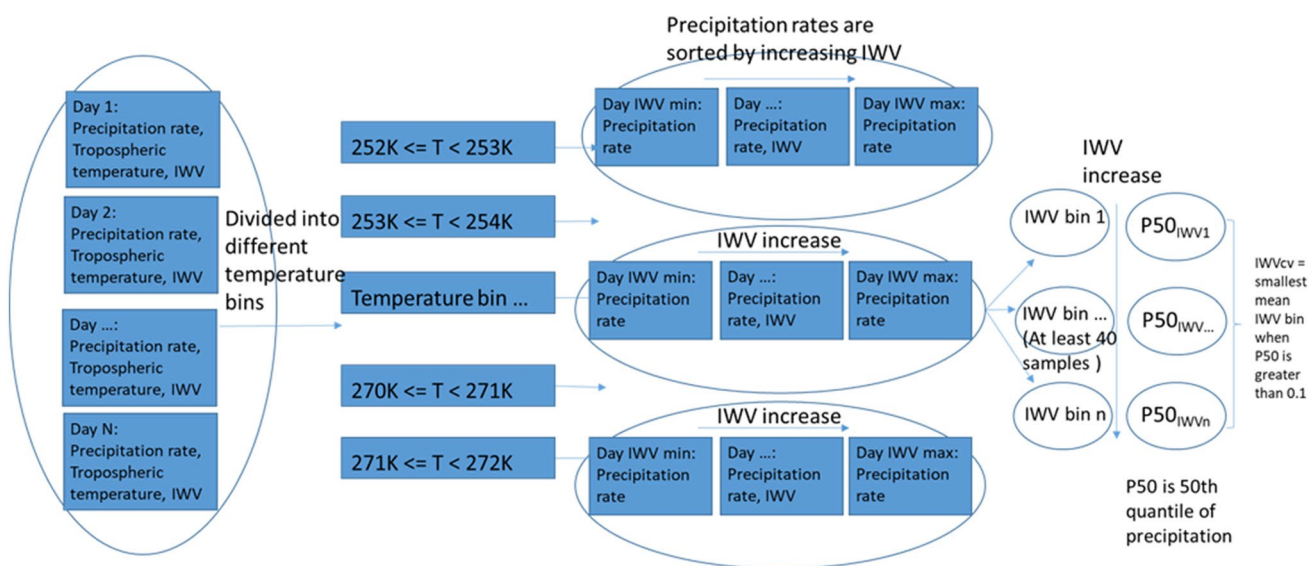


Fig. 2 Method to establish the relationship between temperature, IWV and precipitation (IWVcv)

the sorted IWV values are divided into different bins that contain an equal number of pairs of precipitation rates and IWV to ensure a reasonable number of days to compute the 50th quantile of precipitation. The critical IWV ( $IWV_{cv}$ ) is defined by the mean value of the first IWV bin whose 50th quantile of precipitation is greater than 0.1 mm/day. Here, the 50th quantile of precipitation indicates if there are more precipitating days than non-precipitating days in each IWV bin and shows the transition between mostly non-precipitating days and mostly precipitating days. The probability of exceeding  $IWV_{cv}$  can therefore be used to assess the frequency of precipitation. For the model simulations, the precipitation frequency,  $IWV_{cv}$ , the probability that IWV exceeds  $IWV_{cv}$ , and the probability distribution function (PDF) of IWV rescaled ( $IWV/IWV_{cv}$ ) are computed in the native resolution of each ensemble, and then we average the results of all grid points within the analysis domains to show the final results.

### 3 Occurrence of precipitation

Figure 3 shows the spatial distribution of precipitation frequency (when daily rainfall is greater than 0.1 mm) in winter (DJF) over the Alpine domain for simulations from EUR-44, EUR-11, ALP-11, ALP-3remapEUR-11, ALP-3 and observations. As expected, the difference of resolution between the ensembles and the observations affects this diagnostic, but it is our aim to keep the native resolution here for this comparison. The bias of precipitation frequency between ensembles and observations is shown in Table 4. The spread between simulations in ensembles is shown in Table 5.

Compared to observations, almost all ensembles overestimate on average winter daily precipitation frequency, confirming the results from previous studies obtained with GCMs (e.g. Sun et al. 2006; Dai 2006; Brown et al. 2010). However, we note an improvement with increasing resolution: For EUR-44, it smooths out the variability produced by topographic effects, for example along coastlines, or in valleys around the mountains but the spatial variability is better captured by ALP-3 with a spatial pattern correlation (SPC) of 0.49 and respectively 0.45 for ALP-11, 0.44 for EUR-11 compared to 0.38 for EUR-44. The winter rainfall frequency of EUR-11 and ALP-11 is indeed lower than for EUR-44 over the Mediterranean and mountains (the bias is reduced from 0.11 in EUR-44 to 0.07 in EUR-11 and 0.06 in ALP-11) but quite similar over the plains and about 0.18 for the 3 ensembles. When the convection parameterization is switched off (ALP-3 and ALP-3remapEUR-11), the occurrence is again reduced over the entire domain (bias of 0.03 and 0.05 respectively compared to 0.09 in ALP-11), also over the plains (but still overestimated compared to

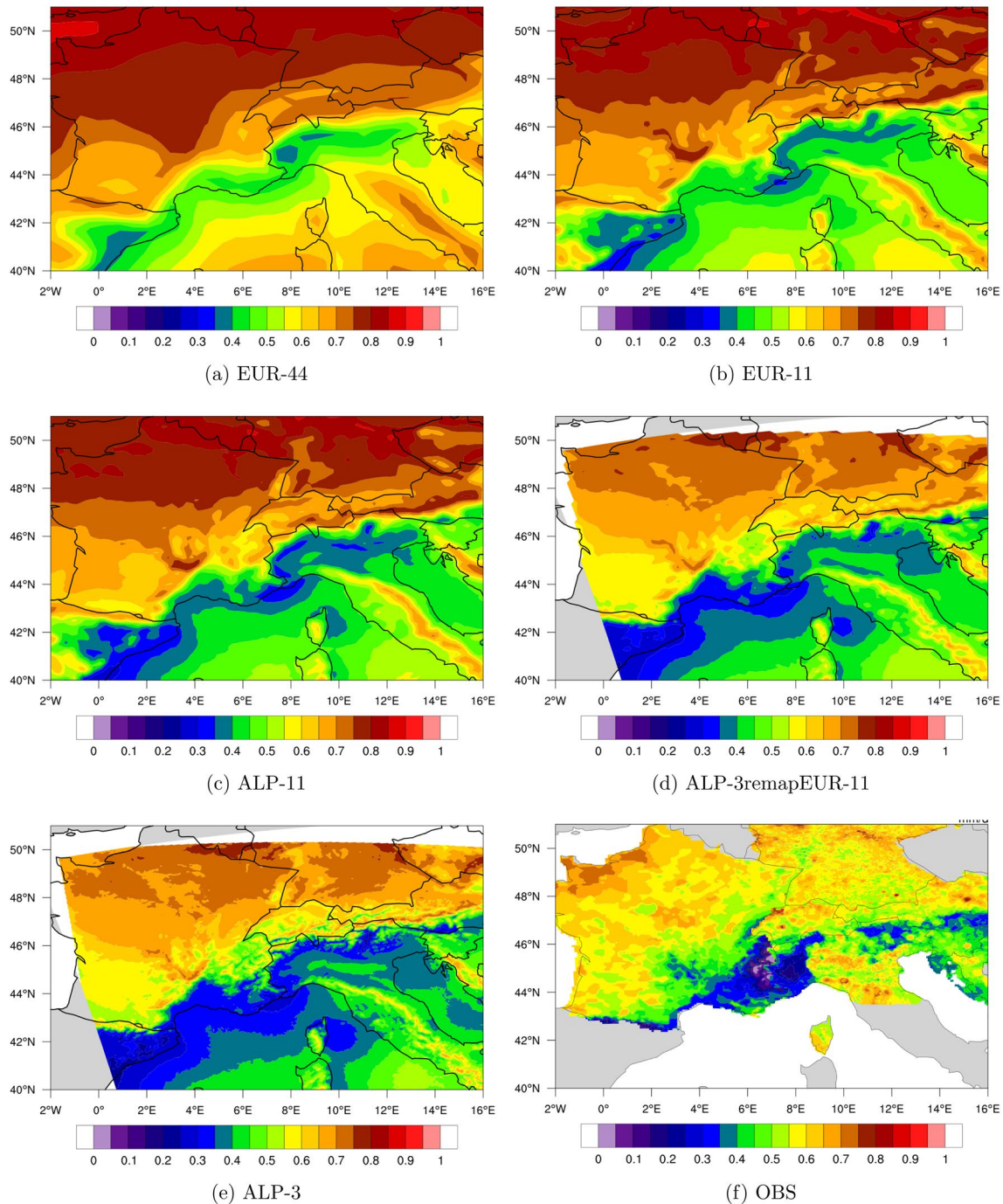
observations, except over the Alpine mountains and Corsica). The higher resolution and explicit convection also reduce the spread between simulations in the ensemble with the standard deviation for the whole evaluation area decreasing from 0.08 for EUR-44 to 0.04 for ALP-3 ensemble.

Figure 4 and the second column in Tables 4 and 5 display the results for summer (JJA). In general, spatial variability in summer is better simulated compared to winter with SPC ranging from 0.63 to 0.77. With a higher resolution, EUR-11 and ALP-11 simulate fewer days of precipitation compared to EUR-44 not only over the sea and mountains as in winter but also over the plains (the bias is 0.06 with EUR-11 and 0.02 with ALP-11, while it is 0.13 with EUR-44). Without convection parameterization schemes, the frequency of summer precipitation in ALP-3 and ALP-3remapEUR-11 ensembles are lower than in EUR-11 and ALP-11 for almost all areas and they even underestimate the occurrence compared to observations (the bias is negative), as already noticed by Ban et al. (2021). In summer over the Alpine region, ALP-11 ensemble is the closest to observations in terms of precipitation occurrence, despite the fact that the resolutions of gridded datasets are closer to the resolution of the ALP-3 ensemble than to ALP-11. Compared to the winter, the spread between simulations in the ensembles is higher with a standard deviation for the whole evaluation area ranging from 0.06 in ALP-3 to 0.14 in EUR-44. However, the spread is still lower when the resolution increases and the convection is not parametrized.

To further investigate the impact of resolution in the precipitation triggering, Fig. 5 shows the precipitation frequency of all the ensembles as a function of IWV and tropospheric temperature over the whole area and 3 selected areas represented on Fig. 1: the whole FPSCONV domain, the Alpine mountains range, the Mediterranean Sea and the continental plains. When surface stations are available in the area, green solid lines indicate the averaged value of IWV as a function of temperature for each station included in the considered area.

For all areas, at low temperature, the range of IWV values for which precipitation occurs is quite narrow (about 6 kg·m<sup>-2</sup>), and a good agreement between the different ensembles and observations is found (green lines in figures represent observed values from stations located within each area). When temperature increases, the range of IWV values becomes larger (greater than 20 kg·m<sup>-2</sup> when the whole range is considered). Values of IWV for rainy occurrence increase at a rate close to Clausius-Clapeyron (hereafter C–C, lower than C–C for the Alpine domain) until a certain value of temperature ( $T_{break}$ ) at which the curve angles away from C–C, as already noticed and discussed in Bastin et al. (2019). Physically,  $T_{break}$  corresponds to the temperature over which the fraction of convective precipitation





**Fig. 3** Precipitation frequency (>0.1 mm/day) in DJF for the different model ensembles and observations: **a** EUR-44; **b** EUR-11; **c** ALP-11; **d** ALP-3 remap on EUR-11; **e** ALP-3; **f** observation

over total precipitation becomes close to 1 and precipitation triggering is thus yielded by conditional instability, which occurs at lower relative humidity rate than saturation.

When considering the whole domain (Fig. 5a, b), we can see that this threshold of IWV value is simulated by the 4 ensembles and visible in the observations over the different stations included in the studied area. The green line with

the lowest values of IWV corresponds to the Caussols station which is located close to the coastline and surrounded by complex terrain (see Fig. 1 and Table 3), where triggering of precipitation is favored by the frequent occurrence of sea breeze which intensifies the upslope winds (Bastin et al. 2006), explaining the occurrence of precipitation for

**Table 4** Bias of precipitation frequency (averaged over all grid points in the different areas shown on Fig. 1) in DJF/JJA between model simulations and observation. Results indicate the MODEL-OBS value, blue shows positive bias and red shows negative bias

Ensemble	Winter (DJF)			Summer (JJA)		
	Alpine mountains	Plains	Whole observation area	Alpine mountains	Plains	Whole observation area
EUR-44	0.11	0.18	0.13	0.10	0.13	0.11
EUR-11	0.07	0.19	0.11	0.00	0.06	0.03
ALP-11	0.06	0.18	0.09	0.03	0.02	0.00
ALP-3remapEUR-11	0.01	0.12	0.05	0.11	0.08	0.09
ALP-3	0.03	0.11	0.03	0.17	0.10	0.12

**Table 5** Standard deviation of precipitation frequency (averaged over all grid points in the different areas shown on Fig. 1) in DJF/JJA from model ensembles

Ensemble	Winter (DJF)				Summer (JJA)			
	Alpine mountains	Plains	Mediterranean	Whole evaluation area	Alpine mountains	Plains	Mediterranean	Whole evaluation area
EUR-44	0.11	0.07	0.1	0.08	0.13	0.14	0.16	0.14
EUR-11	0.05	0.03	0.11	0.07	0.08	0.09	0.15	0.09
ALP-11	0.04	0.03	0.07	0.05	0.06	0.07	0.12	0.08
ALP-3remapEUR-11	0.03	0.04	0.06	0.05	0.06	0.07	0.06	0.06
ALP-3	0.02	0.04	0.06	0.04	0.05	0.07	0.06	0.06

lower values of IWV. This line is however still within the model spread.

The model ensembles clearly simulate T<sub>break</sub> over the Mediterranean and plains. The value of the simulated T<sub>break</sub> over the Mediterranean seems a bit weaker than over the plains (less than 266 K for the sea versus around 268 K in average for the land). Over the Alpine domain, model ensembles do not simulate this limit, while it is visible in the observations (but only from two stations). It can be due to a difficulty of models but also to the locations of the stations which do not necessarily have a good representativeness of the whole Alpine precipitation regime (Lundquist et al. 2019). Also, the values of IWV for which rain occurs are generally lower over the Alpine domain where triggering processes are favored by the complex terrain and because the depth of the atmospheric column is reduced. Generally, the differences between ensembles are not obvious; we can only see higher IWV values for EUR-11 ensemble at low temperatures over the Alpine domain compared to EUR-44 (Fig. 5c).

Entrainment of dry versus moist environmental air into the convective plume conditions the onset of convection (e.g. Wulfmeyer et al. 2016, Kuo et al. 2017; Schiro et al. 2016).

Since parameterization physics treat entrainment differently, we expect to detect differences in the convective transition statistics (see below) between ensembles and among models more than in the temperature break after which convective precipitation dominates. That is why we need to go a step further in the triggering process.

In the next section, we consider IWV<sub>cv</sub> over which the median of precipitation occurrence starts to increase (i.e. when the probability that it rains becomes higher than 50%), and higher probability to exceed IWV<sub>cv</sub>, which is expected to produce higher precipitation frequency. Bastin et al. (2019) pointed out that models which present light precipitation too often generally show lower critical values and higher probability of exceeding them. We also examine the distribution of values around this critical value to better assess the triggering process in the different ensembles and over the different areas. As demonstrated by Kuo et al. (2017), over the tropics (continental and ocean), the enhancement of precipitation with increased IWV only exists when entrainment is strong enough, and the value of IWV<sub>cv</sub> increases with stronger entrainment until a certain value when IWV<sub>cv</sub> ceases to be sensitive to entrainment of environmental air.

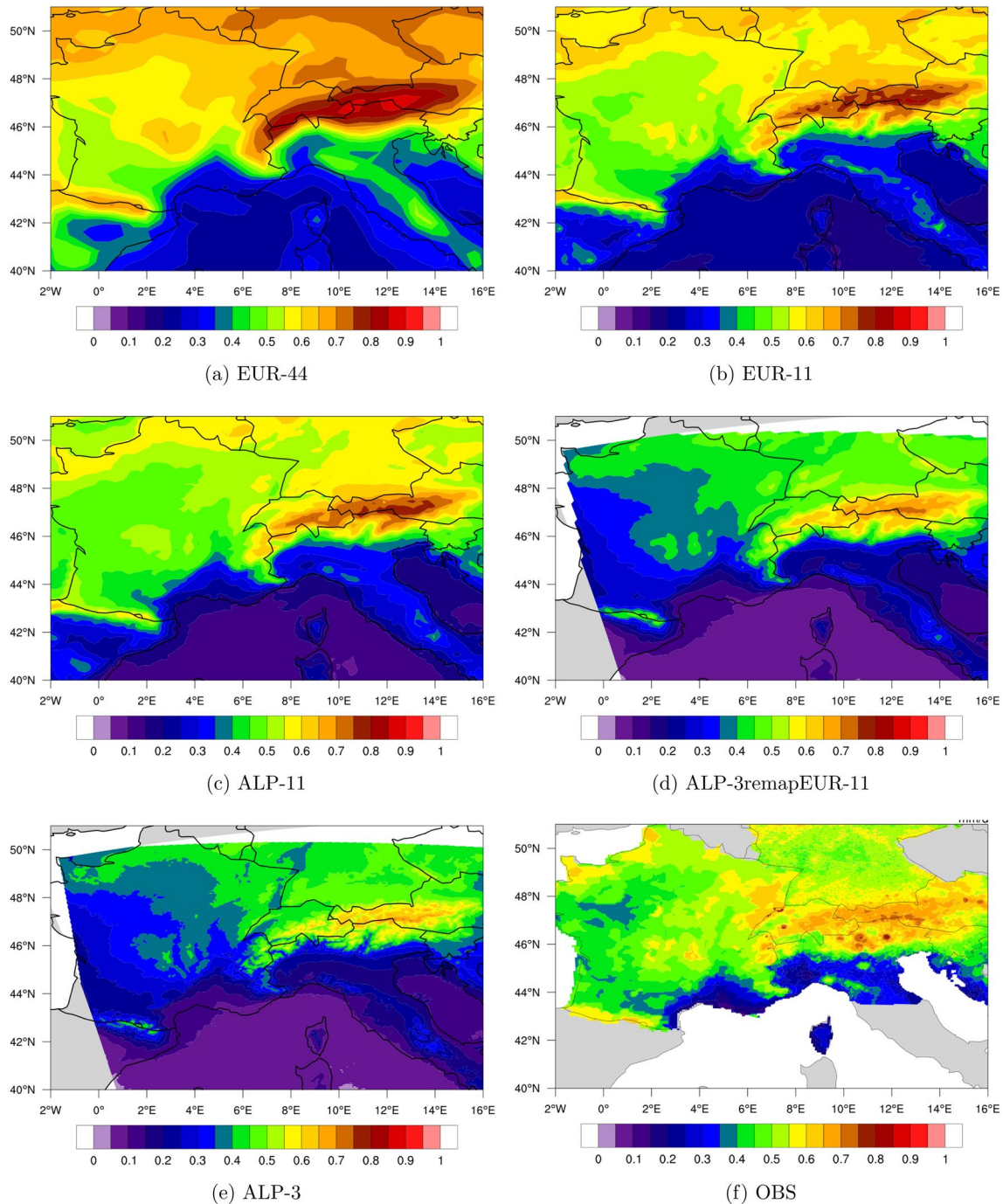


Fig. 4 Same as Fig. 3 but for JJA

## 4 Influence of resolution and convection representation on the triggering of precipitation

### 4.1 Precipitation enhancement

Figure 6 compares the IWVcv from different simulations as a function of tropospheric temperature over: (a) the

FPSCONV domain, (b) Mediterranean, (c) Alpine mountains, and (d) continental plains. The total distribution of IWVcv values for all grid points of evaluation domain and all models is represented by a boxplot, and the mean value of IWVcv for each simulation of the different model ensembles is represented as a filled-color dot. Each color corresponds to a different ensemble: EUR-44 simulations are in blue, EUR-11 simulations in green, ALP-11 in pink,

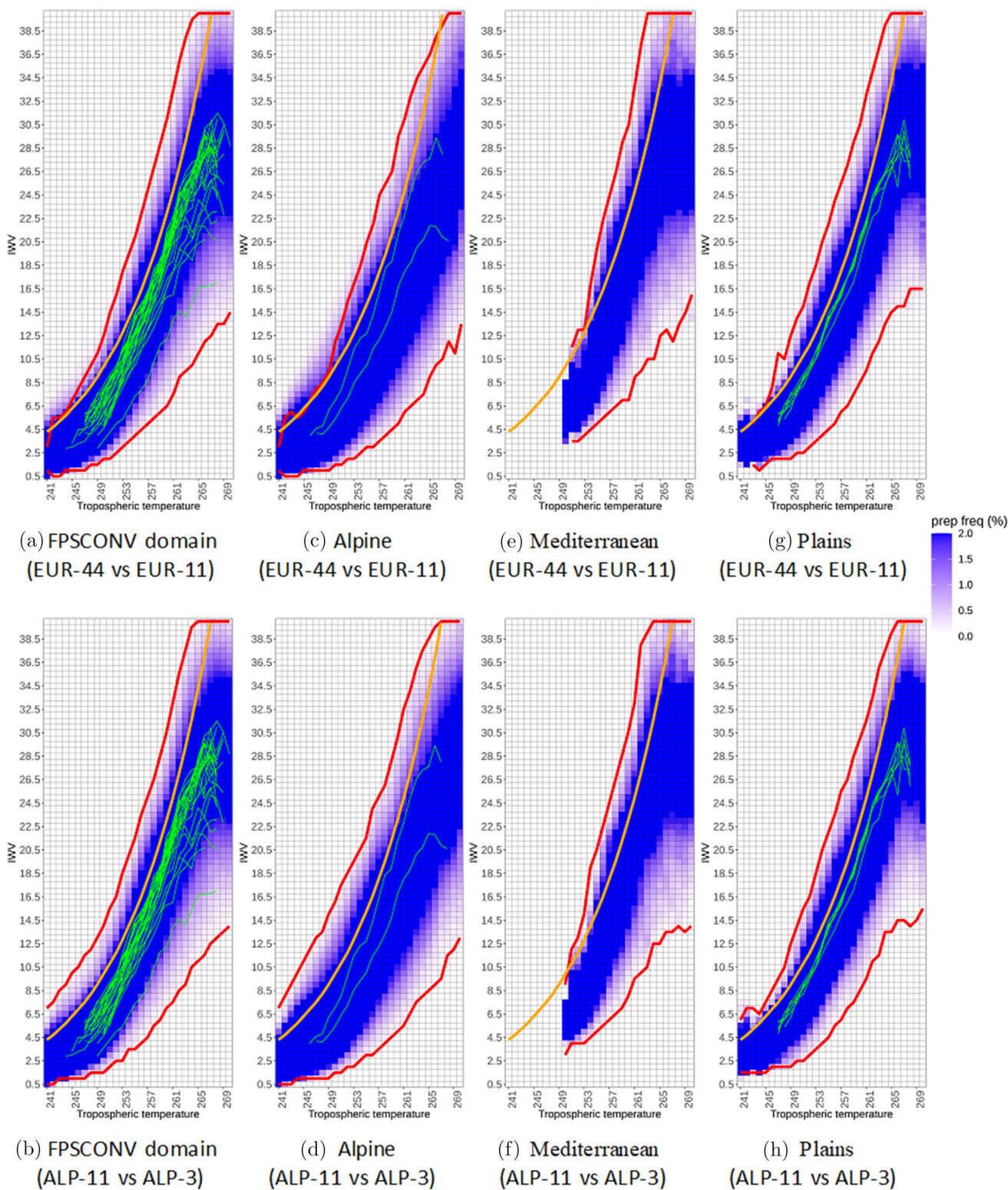


**Fig. 5** Precipitation frequency (%) as a function of IWV and tropospheric temperature over (a, b) whole FPSCONV domain, (c, d) Alpine mountains, (e, f) Mediterranean, and (g, h) plains (see boxes in Fig. 1). The color bars show precipitation frequency for EUR-11 and ALP-3, red lines are the minimum and maximum IWV where precipitation is occurring in EUR-44 and ALP-11. Ensembles are

compared 2 by 2: upper row is for EUR-44 and EUR-11 and lower row is for ALP-11 and ALP-3. Green solid lines show the IWV as a function of tropospheric temperature when it rains from the different stations included in each box. The orange line shows the C-C theoretical saturation humidity as a function of temperature

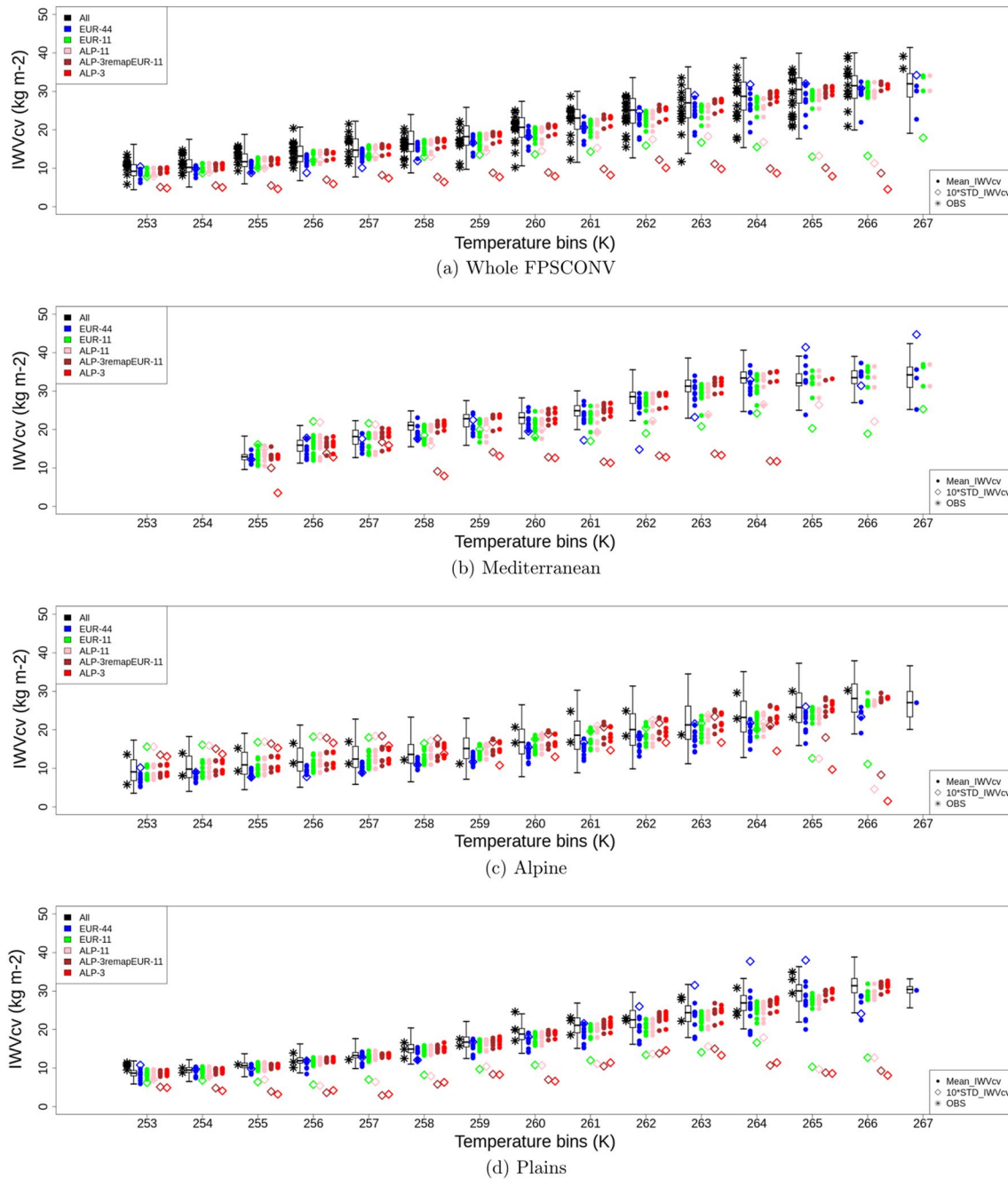


**Fig. 6** IWVcv ( $\text{kg m}^{-2}$ ) from all model's simulations (boxplot), EUR-44 (blue), EUR-11 (green), ALP-11 (pink), ALP-3remapEUR-11 (brown) and ALP-3 (red) over **a** FPSCONV domain, **b** Mediterranean, **c** Alpine mountain and **d** plains. The boxplot denotes the 1%,

25%, 50%, 75%, 99% probability of IWVcv to get this value by considering all grid points and all models used in this study; Black stars represent the observations. See more details in the text

ALP-3remapEUR-11 in brown and ALP-3 simulations in red. The diamonds indicate the standard deviation for each ensemble. It has been multiplied by 10 for a better visualization. The black stars show IWVcv from the observations at the stations which are included in the considered domain. Note the similarity with the range of values from ALP-11 and EUR-11, although ALP-11 ensemble has fewer members

(e.g. Fig. 6a), which suggests that the three different models of the ALP-11 ensemble (with 9 simulations in total) cover an acceptable representation of model variability in this study.

#### 4.1.1 Whole FPSCONV domain

For the whole FPSCONV domain, Fig. 6 clearly shows the increase of IWVcv with tropospheric temperature as well as the increase of the spread between models, the interquartile range of the total distribution being  $2.8 \text{ kg.m}^{-2}$  for the lower temperature bin, and being around  $7.5 \text{ kg.m}^{-2}$  for the higher temperature bin. As in Fig. 5, IWVcv does not increase any further beyond a certain temperature (above about 265 K), and we can see that Tbreak over the sea is lower than over the land. Concerning observations, most of the IWVcv values for the observed stations are contained within the model boxplot range. For lower temperatures, most mean IWVcv values from EUR-11 simulations are equal or higher to those from EUR-44 simulations (difference of the ensemble mean is about  $0.5 \text{ kg.m}^{-2}$ ) and the spread between models (represented by the standard deviation as diamonds in the figure) is similar. At higher temperatures, the difference between IWVcv ensemble mean values increases, and the standard deviation becomes very large in EUR-44 ensemble. Standard deviation of EUR-11 simulation is lower than EUR-44 simulation by about  $1.9 \text{ kg.m}^{-2}$  in the 265 K temperature bin. However, it is important to note that we are considering several extra independent models in EUR-44 (UCLM, RACMO22E, HadRM3P) with respect to EUR-11. This extra model diversity can influence the value of the standard deviation. For the other ensembles, mean values of IWVcv for ALP-3 simulations are higher than for ALP-11 in all temperature bins, suggesting that higher resolution increases the value of IWVcv. This difference becomes larger at high temperature, when convective processes become predominant, and the convection parameterization schemes become more important. Since ALP-3 has both higher resolution and a different representation of convective processes, it is suspected that it is not only the resolution which affects the IWVcv value. Indeed, ALP-3remapEUR-11 has very similar values to ALP-3 and higher than ALP-11, although the resolution of the ALP-3remapEUR-11 is similar to that of the ALP-11. The fact that the standard deviation is not much different between ALP-3 and ALP-3remapEUR-11 simulations and lower than in ALP-11 also confirms that activation of convection parameterization schemes contributes to increased spread between models because of the inherent assumptions in convection parameterization schemes.

When considering the probability of exceeding IWVcv (Fig. 7), the models' deficiencies in their ability to represent the distribution of humidity is evident. Indeed, the mean probability decreases when temperature increases but the range is quite large for both low and high temperatures, which reveals the difficulty for models to correctly simulate the distribution of critical humidity throughout the column at all temperatures, not only when convection is active and

when surface processes are important. Most of the observations show lower probability to exceed the threshold than the medium of boxplot at low temperature and the mean of each model at all temperature bins. It has already been noticed that models generally overestimate low values of humidity (Bastin et al. 2019; Ning et al. 2013) and do not perfectly simulate the phasing of the diurnal cycle (Ning et al. 2013) and the threshold of IWV values observed at high temperature (Bastin et al. 2019). However, some differences between ensembles exist: In EUR-44 ensemble, some models do not really capture IWVcv well because they too frequently exceed IWVcv threshold. At low temperature, EUR-11 simulates probability lower than EUR-44 but the spread is not much different showing a similar degree of agreement between models of each ensemble. At high temperature bin (265 K), the probability in EUR-11 is not lower than EUR-44 but the spread reduces more significantly showing a larger similarity among models response at higher resolution. When convection parameterization schemes are switched off, ALP-3 and ALP-3remapEUR-11 simulate probability to exceed IWVcv lower than ALP-11 and the standard deviations are lower, too. At high temperature bins, we cannot see a big difference between ALP-3 and ALP-3remapEUR-11, which means that the impact of convection representation is likely more important in these bins. Although higher IWVcv is expected to produce lower probability to exceed IWVcv, the probability is both linked to the value of IWVcv itself, and to the moisture content. Surface humidity can strongly help to spend more time close to the critical value because the surface provides lots of moisture through latent heat flux but does not affect the critical value itself.

To better understand the role of resolution versus the role of convection parameterization, the results over the three different areas are analyzed: over the sea, neither resolution nor convection representation should matter a lot, since the triggering process of precipitation is mainly linked to large scale forcing such as mesoscale cyclonic systems which are mostly developed by baroclinic instability and affected by diabatic processes similar to other extratropical cyclones in the mid-latitude storm track (Nuissier et al. 2011; Flaounas et al. 2022). Over Alpine topography, resolution should be predominant and over the plains both are expected to matter.

#### 4.1.2 Mediterranean sea

What we obtain over the Mediterranean (Figs. 6b and 7b) confirms what we expect: for similar temperature, IWVcv over the sea is higher than over land because of less convective processes (Lucas et al. 1994), so cloud formation needs more humidity in the lower layer to overcome the saturation deficiency of the lower free troposphere, which increases when temperature increases.

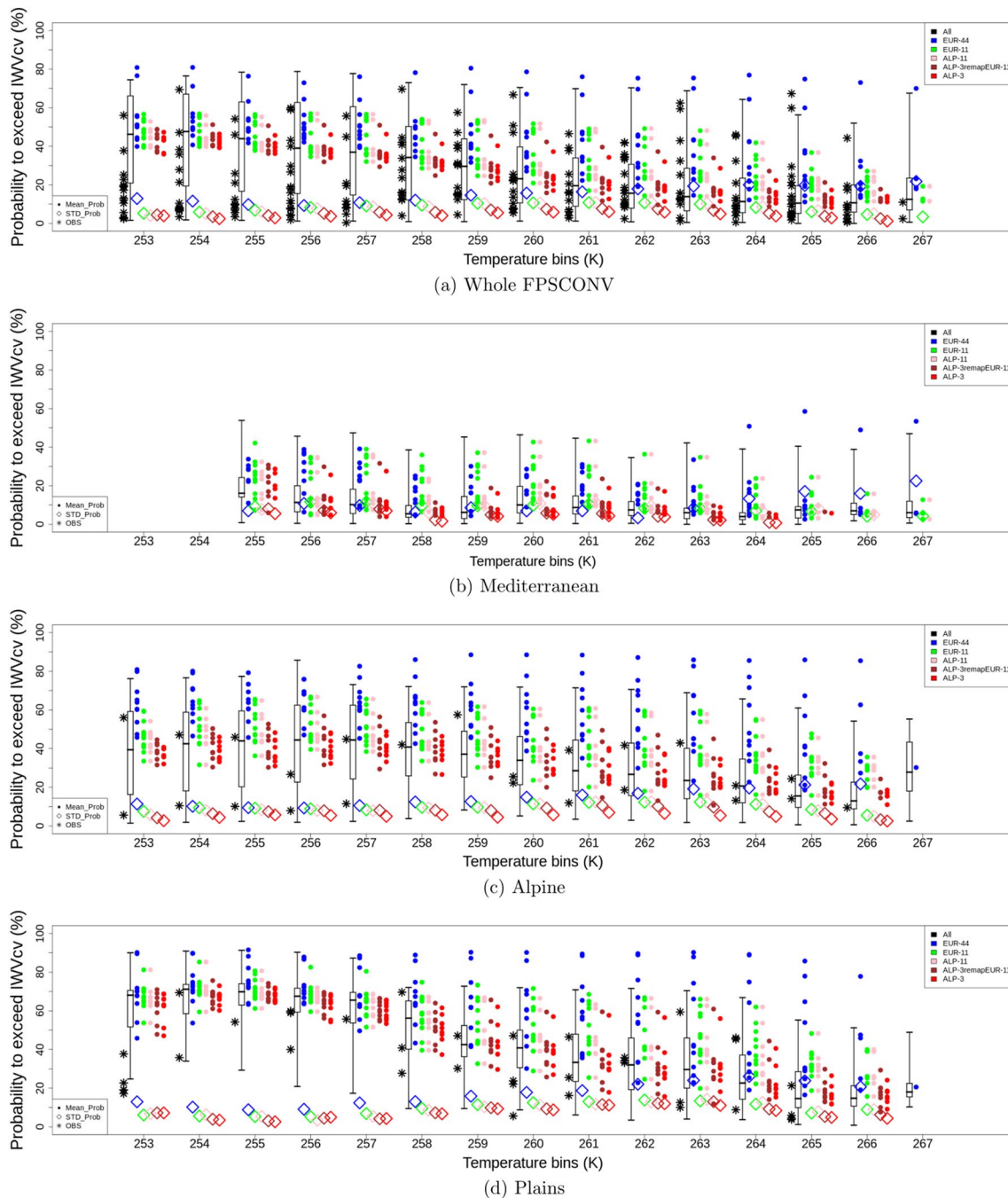


**Fig. 7** Same as Fig. 6 but for probability to exceed IWVcv (%), the diamonds only show the standard deviation for each ensemble and have not been multiplied by 10

The impact of model resolution on the values of IWVcv is not clear. EUR-11 and ALP-11 indeed simulate lower values of IWVcv than both EUR-44 and ALP-3, while ALP-3 values are within the range of EUR-44. But the spread between models is reduced when convection parameterization is switched off.

Figure 7b shows that the probability to exceed the IWVcv does not depend on temperature, which is consistent with

the fact that convection is generally weak over the sea, the main process of lifting being the large scale convergence of moisture, which does not depend on temperature. And as for IWVcv, it does not show a sensitivity to resolution while switching off convection parameterization decreases the probability to exceed the critical value (probably because the critical value is larger) and decreases the standard deviation between models.

### 4.1.3 Alpine domain

Over the Alpine mountains (Fig. 6c), IWV<sub>cv</sub> increases at a lower rate than over other areas but does not stop increasing. The absence of a T<sub>break</sub> value can be explained by the fact that topographic lifting is strong enough to ensure that saturation is reached independent of temperature. With increased model resolution, the mean value of IWV<sub>cv</sub> in EUR-11 is higher than in EUR-44 for all tropospheric temperature bins, while the spread becomes smaller at higher temperatures. This suggests that resolution significantly impacts the value of IWV<sub>cv</sub> over mountains compared to other areas. This is because dynamical processes linked to orography play an important role in triggering convection. When considering ALP-11, ALP-3remapEUR-11 and ALP-3, we can detect some differences between the three ensembles with, once again, higher values of IWV<sub>cv</sub> for ALP-3 than for ALP-11. At higher temperatures, when comparing the mean value of IWV<sub>cv</sub>, there is a much bigger difference between ALP-11 and ALP-3remapEUR-11 than between ALP-3 and ALP-3remapEUR-11. However, the fact that we detect differences between ALP-3 and ALP-3remapEUR-11 confirms that over mountains, data resolution impacts the diagnostics and that we should be careful to use gridded datasets that have consistent resolution and use representative stations to evaluate models (Lundquist et al. 2019). However, we cannot exclude the impact of convection representation on IWV<sub>cv</sub> in the simulations beside increasing model resolutions.

Higher resolutions result in lower probabilities and standard deviations in almost all temperature bins (Fig. 7c). With convection permitting simulations, the probability to exceed IWV<sub>cv</sub> is lower and differences between ALP-3remapEUR-11 and ALP-11 are larger than between ALP-3 and ALP-11. However, we still cannot really conclude on the impact of switching off convection schemes compared to resolution at higher temperature because we are aware that ALP-3remapEUR-11 simulation is not equivalent to performing a simulation with explicit convection at 0.11° resolution.

### 4.1.4 Plains

Over the plains (Fig. 6d), when increasing model resolutions, the value of IWV<sub>cv</sub> in EUR-11 is not really increased compared to EUR-44 but the spread is reduced significantly between models. When considering ALP-11, ALP-3remapEUR-11 and ALP-3, we can see a bigger impact of convection representation, with very similar results for ALP-3remapEUR-11 and ALP-3, and significant differences with ALP-11.

At lower temperatures, increasing resolution does not reduce the probability to exceed IWV<sub>cv</sub> but the spread between models decreases a little in EUR-11 compared

to EUR-44 (Fig. 7d). At higher temperature bins, both the impact of resolution and the impact of convection representation become more effective.

To conclude this section, when considering the whole domain, if we only increase model resolution, the values of IWV<sub>cv</sub> are not higher for every model but it can help to reduce the uncertainty between different models. But with convection-permitting simulations, the value of IWV<sub>cv</sub> is increased everywhere and the spread is lower in all temperature bins, especially in higher temperature bins. As shown in Fig. 4, this impacts the occurrence of precipitation, which becomes too infrequent in summer compared to available observational datasets. However, high resolution simulations can be more credible than gridded datasets over topography as suggested by Lundquist et al. (2019). Resolution does not impact the results substantially over the sea but is more important over mountains where the processes of convective triggering are linked to orography. The more significant effects of higher resolution on precipitation triggering over the Alps are consistent with previous studies by Knist et al. (2020) and Fosser et al. (2015). We cannot exclude the effect of explicitly resolved convective processes over the Alpine mountains. Some other studies show that it is both the reduced grid spacing and explicit convection schemes in CPMs that improve the simulation of precipitation over the Alps (Bauer et al. 2011, Adinolfi et al. 2021; Ban et al. 2014; Giorgi et al. 2016; Hohenegger et al. 2008; Keller et al. 2016; Langhans et al. 2013; Leutwyler et al. 2017; Lind et al. 2016; Lüthi et al. 2019; Reder et al. 2020). An increase in the resolution may even play a role in improving the timing of the diurnal cycle and intensity of convective precipitation (Prein, et al. 2013) or precipitation triggering in winter (Piazza et al. 2019) over the Eastern Alpine region. Although the deactivation of convection parameterization does not show a clear effect on IWV<sub>cv</sub> over mountainous areas except at higher temperatures, it should be an important argument regarding temperature evolution over the Mediterranean. According to the results obtained over the tropics by several studies (Kuo et al. 2017), entrainment may explain part of the differences obtained here but it is difficult to extract the information from ensemble experiments.

In addition, summer or winter precipitation occurrence is strongly related to atmospheric circulation. Winter and summer atmospheric circulations which influence Europe are often classified into four main weather regimes (WR; e.g. Corti et al. 1999; Yiou et al. 2008): In summer, the positive phase of North Atlantic Oscillation (NAO+) and Scandinavian Blocking (BLO) yield an anticyclonic circulation over western Europe, while the negative phase of NAO (NAO-) and Atlantic Ridge (AR; also called Greenland Anticyclone) favor cyclonic circulation (Yiou et al. 2008). In winter, over northern Europe, NAO+ (resp. NAO-) is associated with rather warm (cold) temperature and more (less)



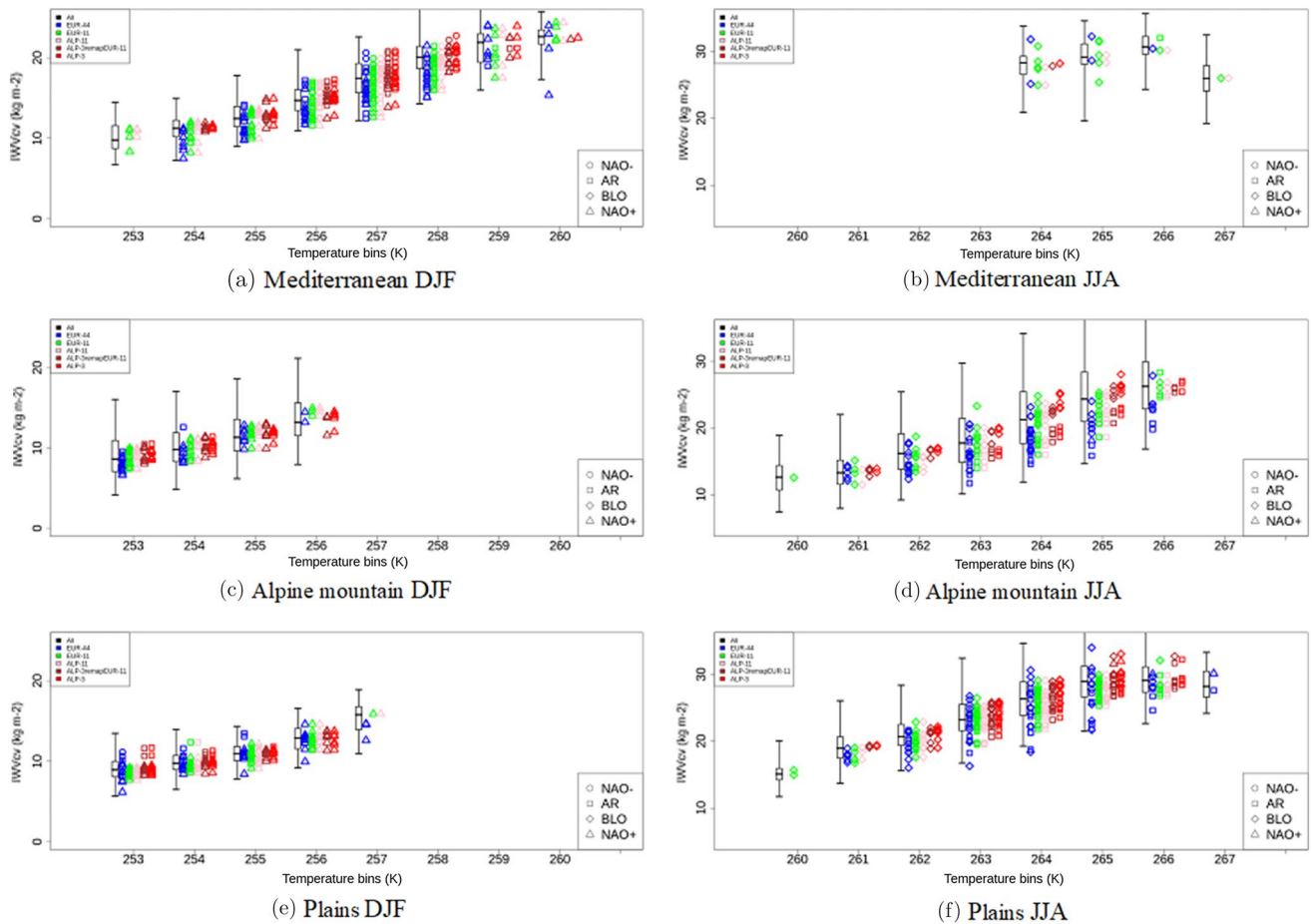


**Fig. 8** IWVcv ( $\text{kg}\cdot\text{m}^{-2}$ ) from all model's simulations (boxplot), EUR-44 (blue), EUR-11 (green), ALP-11 (pink), ALP-3remapEUR-11 (brown) and ALP-3 (red) over Mediterranean (a, b), Alpine mountain (c, d) and plains (e, f). The boxplot denotes the 1%, 25%, 50%, 75%,

99% probability of IWVcv to get this value by considering all grid points and all models used in this study; Circles represent IWVcv under NAO- weather regime; Squares for AR; Diamonds for BLO and triangles for NAO+

precipitation, and blocking with cold and dry weather (e.g. Cattiaux et al. 2010). Over southern Europe, precipitation is increased under NAO- conditions, while droughts are more frequent under NAO+ (Yiou and Nogaj, 2004). To investigate the relationship between the IWV and precipitation under lower and higher tropospheric temperature by taking into account the impact of atmospheric circulations, we separate the results between these four WRs in Figs. 8 and 9. Moreover, triggering of convective precipitation strongly depends on the atmospheric stability. In this study, due to the lack of all necessary variables to estimate stability, we used the difference between potential temperature at 850 hPa and near surface temperature at 2 m as a stability index. It should be noted that this difference cannot fully represent the atmospheric stability but it can feature partly some aspects of it. The more negative the difference, the more unstable the atmosphere. Figure 10 shows this index as a function of tropospheric temperature over Mediterranean (a), Alpine

mountain (b) and plains (c) in JJA for the different WRs, when it rains.

The NAO is the leading mode of winter seasonal mean circulation variability in the Europe–Mediterranean region (Seager et al. 2020). During the positive phase of NAO, the increased difference in pressure between the high pressure system centered over the Azores islands and low pressure system centered over Iceland results in a stronger Atlantic jet stream and a northward shift of the storm track. It establishes low-level southwesterly flow, bringing warm air over northern Europe, and a northerly flow over southern continental Europe. Consequently, northern Europe experiences increased storminess and precipitation due to the enhanced south-westerlies meeting topography. Below-normal precipitation occurs over southern continental Europe and the Mediterranean region under the influence of subsiding air and mean flow moisture divergence (Seager et al. 2020). Figure 8a shows that over the Mediterranean, for intermediate temperature bins, it rains under three WRs (NAO+,

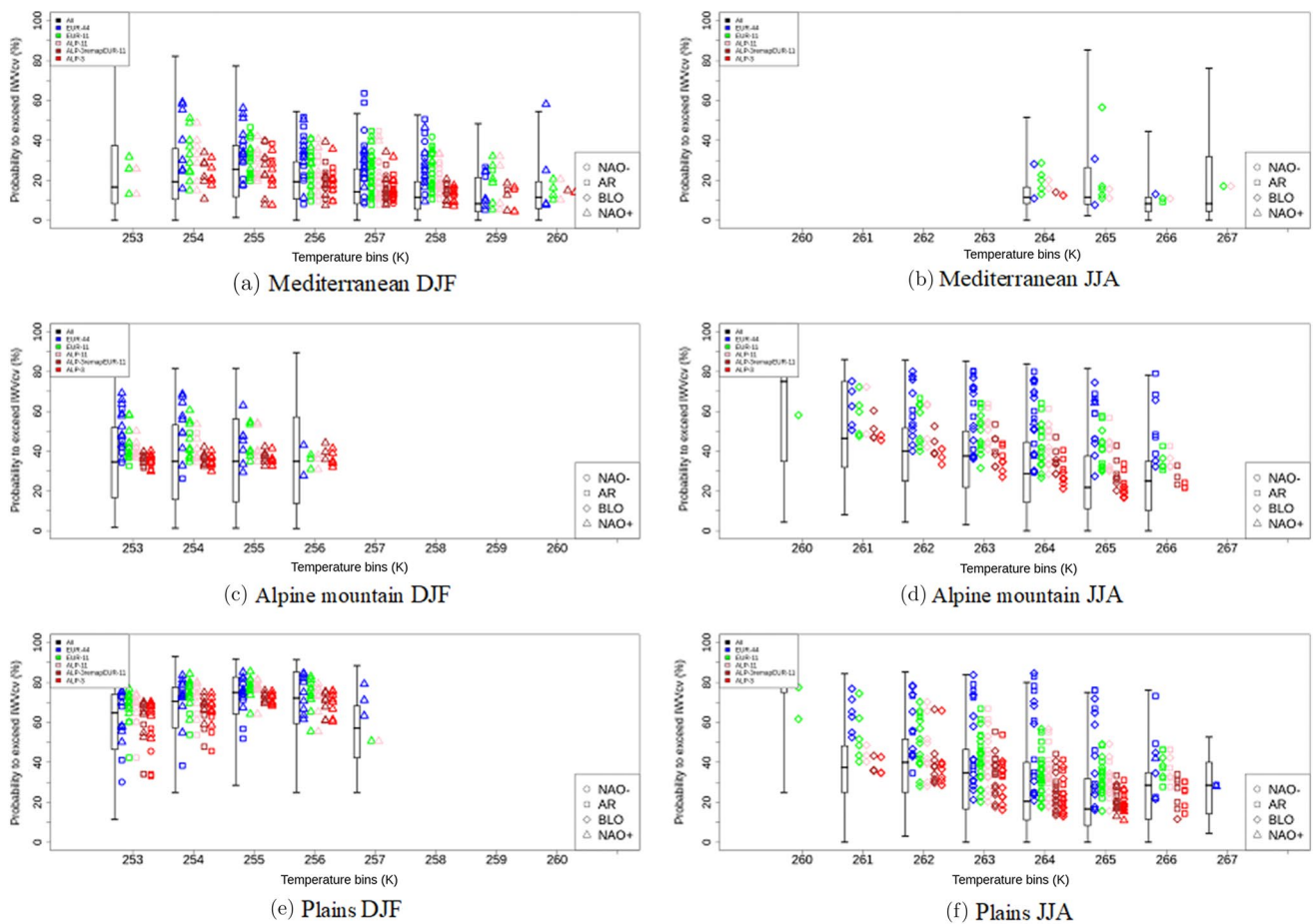


**Fig. 9** Same as Fig. 8 but for probability to exceed IWVcv (%)

NAO- and AR), with a big spread of values of IWVcv, but the higher values of IWVcv being obtained for NAO- in bins 257 and 258 K for all ensembles but EUR-44 in bin 258 K. This high value of IWVcv indicates that the atmosphere contains more water when it starts to rain, and it is consistent with the finding of Yiou and Nogaj (2004) who showed that the most extreme rain events occur during NAO- over southern Europe. More surprisingly, at lower and higher temperature bins, winter precipitation over the Mediterranean occur under NAO+ regime, which is not what was expected by previous studies, and the values of IWVcv for these bins are more sensitive to the convection representation than to resolution. However, NAO+ is also the dominant regime of precipitation over the Alps and the plains (Fig. 8c, d), and values of IWVcv are lower than over the Mediterranean. This is in good agreement with previous studies showing that precipitation over the northern Europe is more frequent than over southern Europe under NAO+ regime, and leading to lower IWVcv and higher probability to exceed IWVcv (Fig. 9) over the land compared to the Mediterranean. It is interesting to note that neither resolution or convection representation strongly affect the value of IWVcv over Alps

and plains, but the explicit convection strongly decreases the probability to exceed the critical value for most temperature bins and more strongly over the Alps. Beside NAO circulation, AR also contribute to winter precipitation over the Plains but with lower probability to exceed the critical value (Fig. 9e).

During summer, over the Mediterranean, the only WR when it rains is blocking (Fig. 8b). Blocking conditions are usually not favorable for precipitation. However, the strong low-level instability shown on Fig. 10a can explain the possibility to have rain in model simulation under this WR despite the subsidence. The high IWVcv illustrates the fact that triggering process in summer necessitates a strong lifting of particles, and the probability of exceeding IWVcv (Fig. 9b) is very low due to less convection over the sea. Over the plains and the Alpine mountain, precipitation occurs mostly under BLO and AR regimes. The values of IWVcv are higher in BLO and lower in AR regime, which is consistent with anti-cyclonic (BLO) versus cyclonic (AR) conditions, this later regime favoring large-scale precipitation while convective precipitation dominates for BLO. The convective triggering is indeed explained by stronger instability under BLO

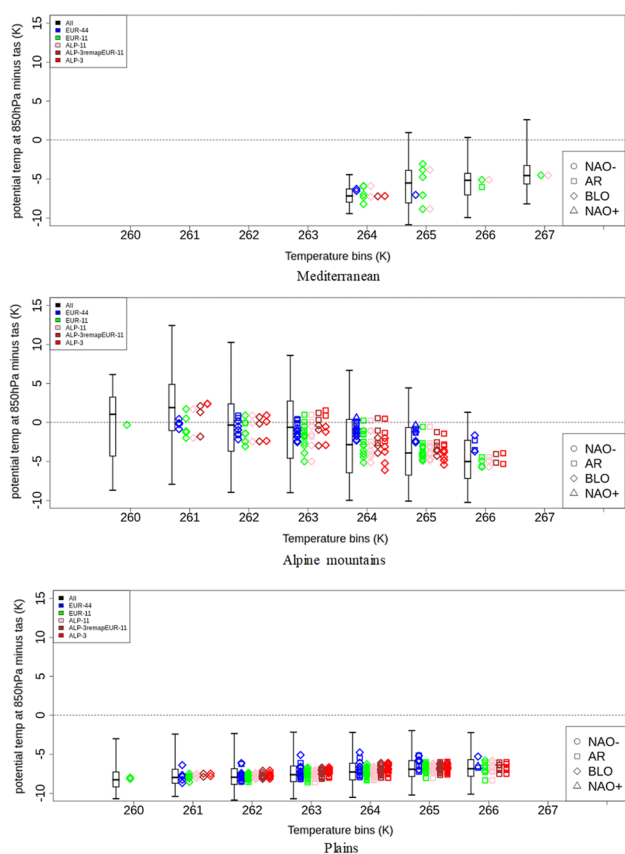


**Fig. 10** Difference between potential temperature at 850 hPa and near surface temperature at 2 m (K) in the summer from all model's simulations (boxplot), EUR-44 (blue), EUR-11 (green), ALP-11 (pink), ALP-3remapEUR-11 (brown) and ALP-3 (red) over Mediterranean (top), Alpine mountain (middle) and plains (bottom). The boxplot denotes the 1%, 25%, 50%, 75%, 99% probability of IWV<sub>cv</sub> to get this value by considering all grid points and all models used in this study; Circles correspond to NAO- weather regime; Squares are for AR; Diamonds for BLO and triangles for NAO+

conditions (Fig. 10). In addition, IWV<sub>cv</sub> over the Alpine mountain (Fig. 8d) is lower than over the plains (Fig. 8f) in the same WR and temperature bin due to the effects of topography. Less instability is needed to trigger convection over the Alps, as indicated on Fig. 10. It is also interesting to note that the vertical temperature gradient is not very sensitive to resolution or convection representation over the plains (Fig. 10 bottom), while strong differences between ensembles exist for the probability to exceed the critical value (Fig. 9), whatever the WR.

## 4.2 Distribution of occurrence of IWV

Several studies (e.g. Neelin et al. 2009; Sahany et al. 2014) suggest that the shape of the distribution of IWV near and above IWV<sub>cv</sub> may be a robust indicator of transition to deep convection over the tropical oceans and can be useful

in integrating properties of various statistical measures of precipitation. Figures 11 and 12 show the number of occurrences (units) of IWV rescaled by the corresponding critical values for each of the temperature bins, considering only the precipitating days for the period from 2001 to 2008. Figure 11 is for the whole domain, for the model ensembles ALP-11 and ALP3remapEUR11 and for observations (all stations are considered in order to generate sufficient sample size). Figure 12 presents the results for each box separately only for the two above-mentioned model ensembles because of insufficient sampling when observations are restricted to few stations. The occurrence for each area is calculated by averaging all grid points in that box.

In general and in consistency with previous studies (e.g. Neelin et al. 2009; Sahany et al. 2014), the occurrence of IWV for precipitating days features a peak around IWV<sub>cv</sub> (Fig. 11a, b). Compared to observation (Fig. 11c), models tend to simulate higher IWV occurrence, consistent with the fact that models tend to overestimate precipitation frequency. However, the highest peak in the IWV distribution occurs around the IWV<sub>cv</sub> for both observation and models, except for the 264 K temperature bin. The models simulate precipitation at values of IWV above IWV<sub>cv</sub> more often than for observations, but the overestimation seems to decrease with explicit convection. The shapes of the distributions look quite similar between the parametrized and explicit convection ensemble with very few differences between temperature bins below IWV<sub>cv</sub>—except above the Mediterranean Sea (Fig. 12c, d)—and larger differences between temperature bins after IWV<sub>cv</sub>, with a more abrupt decrease of occurrence at high temperature than at low temperature. However, we can note some differences between the two ensembles: over the high mountain and the plains (Fig. 12a, b, e, f), maximum of IWV counts for precipitation days occurs when IWV exceeds IWV<sub>cv</sub> in ALP-11 simulations, while without convection parameterization schemes, it is the highest around IWV<sub>cv</sub>. For both ensembles, after the highest frequency is reached, IWV occurrence decreases at a higher rate for higher temperature bins but the decrease is sharper in ALP3remapEUR11 than in ALP-11 simulations. The fact that the maximum of IWV count for precipitation days occurs at higher rescaled IWV values and that the rate of decrease after the maximum is weaker in ALP-11 ensemble suggests weaker dissipative effects when convection is parametrized (Holloway and Neelin, 2009).

Over the Mediterranean, the distributions peak at IWV<sub>cv</sub> for both ensembles and all temperature bins, but they are much sharper than over the other domains (Fig. 12c, d). Important differences appear between temperature bins, with flatter distribution at higher temperature bins in both ensembles but much more pronounced in ALP3remapEUR11 ensemble. This flattening is the result of strong saturation deficit (Seager et al. 2015) at higher temperatures without

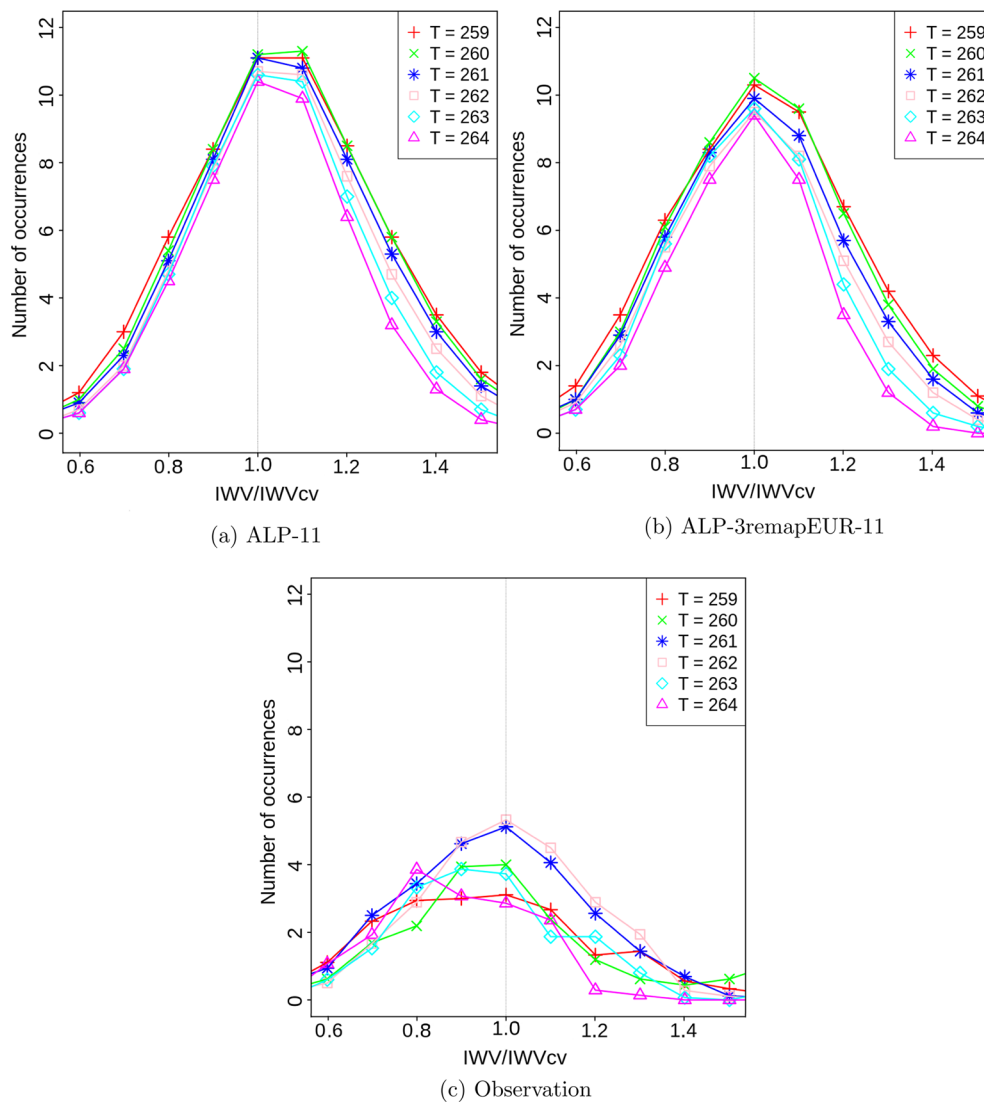


**Fig. 11** Number of occurrence (units) of IWV rescaled by the corresponding onset threshold values  $IWV_{cv}$  for precipitating days between ALP-11 (a), ALP3remapEUR11 (b) and observation (c) over the FPSCONV domain

triggering effects over the sea, so we do not have enough precipitating days to plot the distribution for the highest temperature bins in ALP3remapEUR11 ensemble. More specifically, over the sea (Fig. 12c, d), more precipitation occurs at lower  $IWV_{cv}$ , and the asymmetry of the distribution below and above  $IWV_{cv}$  is the opposite to the one exhibited over mountains or plains (Fig. 12a, b, e, f). Over the sea, precipitation triggering is determined by large-scale dynamics operating on longer time scales (Xoplaki et al. 2003; Trigo et al. 2006), so the frequency of occurrence is higher below  $IWV_{cv}$  and is not constrained by loss of water vapor by precipitation processes. In contrast, convective precipitation processes are determined by short time and small space scales over the land, at higher temperatures when the critical value and the associated precipitation pickup are a property

of the convection itself, depending only on the tropospheric water vapor and temperature (Holloway and Neelin, 2009). So  $IWV_{cv}$  plays an important role for precipitation triggering and a larger fraction of precipitation occurs around  $IWV_{cv}$ .

### 5 Concluding remarks

This work uses different model ensembles from EURO, Med-CORDEX and CORDEX FPS -« Convective phenomena at high resolution over Europe and the Mediterranean» to investigate the impact of model resolution and convection representation (parameterized versus explicit) in simulating precipitation frequency over Europe and the Mediterranean.

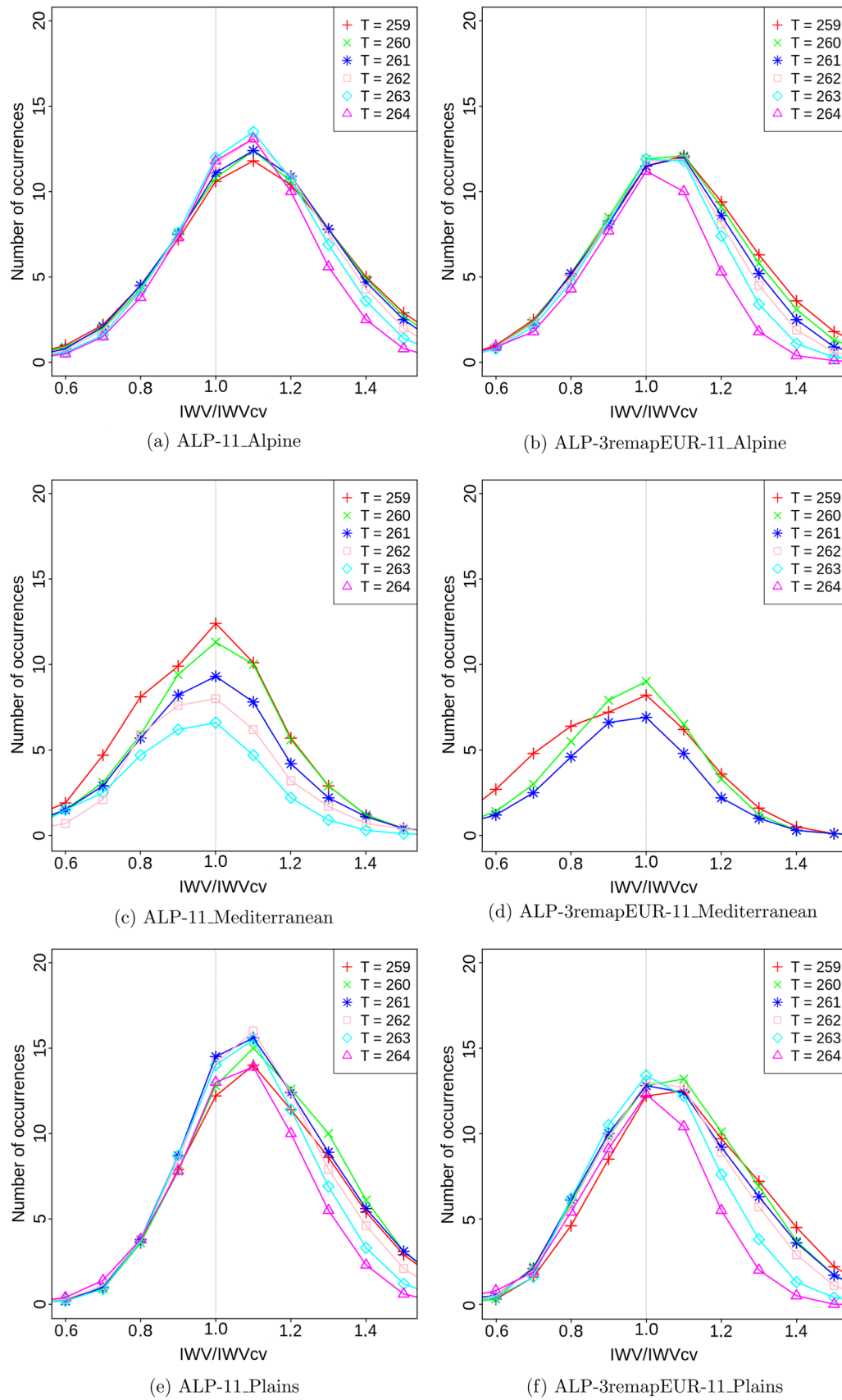


**Fig. 12** Same as Fig. 8 but for ALP-11 (left), ALP3remapEUR11 (right) over the Alpine mountain (a, b), Mediterranean (c, d) and plains (e, f), respectively

We investigate the differences between the model ensembles by focusing on triggering processes. In this study, precipitation is considered in the relationship with tropospheric temperature and IWV, which has been shown to be a better proxy of deep convection onset than saturation over tropical oceans (e.g. Neelin et al. 2009; Sahany et al. 2011) as well as over Europe (Bastin et al. 2019).

The results indicate that with higher resolution, models simulate fewer precipitating days in both summer and winter. Precipitation frequency is reduced in CPMs without convection parameterization schemes, and even becomes lower than the observations (other simulations overestimate precipitation frequency) in summer. This result has been noticed in previous studies (e.g. Ban et al. 2021; Berthou et al. 2020). For example, Ban et al. (2021) have pointed out that the FPS-CONV ensemble includes lots of WRF simulations with common configuration showing a summer dry bias which then has a strong weight in the ensemble mean. In the ensemble we consider here, 6 over 9 simulations use this WRF configuration. The absence of a deep convection parameterization is of course another possibility: some of the models are run for the first time at such a high-resolution and no prior calibration or tuning has been performed, in particular for the horizontal diffusion and the time step which have been shown to be important for deep convection processes in COSMO model at this resolution (Zeman et al. 2021). The other parameterizations that are still activated in CPRCMS can also explain the dry bias, in particular the microphysics scheme and the land surface models: In their study, Berthou et al. (2020) show that at higher resolution, when the top layer of soil is saturated, excess of water disappears into the surface run-off whereas it is drained into the second layer at lower resolution; it leads to dry soil conditions which tend to be associated with lower moist static energy (MSE) per unit of planetary boundary layers (PBL) air and thus with a reduced potential for convective development. But here we show that the less frequent occurrence of precipitation is not only explained by higher temperatures in CPMs (e.g. Sangelantoni et al. submitted) but also by a higher critical value of IWV (IWV<sub>cv</sub>) that must be reached to trigger precipitation at similar temperatures, and a lower probability of exceeding this critical value. Moreover, in CPM simulations, it is shown that the occurrence of precipitation is more peaked around the critical value, indicating stronger dissipative effects than when convection is parametrized. This reduces the occurrence of rainfall and this effect will likely be more pronounced when we will consider hourly time scales in the next study. Finally, the spread between models in simulating IWV<sub>cv</sub> and its exceedance probability is reduced in the ensemble of models with explicit convection over land, especially at higher temperatures, when fraction of convective precipitation to total precipitation becomes more important. This is likely because inherent assumptions in convection

parameterization schemes (different expressions of entrainment and convective updrafts) alter the statistics for the transition to deep convection (Kuo et al. 2017; Tompkins 2001).

Considering the Alpine mountains, model resolution has a larger impact than over other areas in simulating IWV<sub>cv</sub> because dynamical processes linked to orography play an important role in triggering convection. However, we cannot completely exclude the influence of convection parameterization schemes. Over the plains, both model resolution and convection representation affect the precipitation triggering, especially at higher temperatures. Some studies have shown that in CPMs, land surface/atmosphere interactions are modified compared to RCMs with drier soils and weaker latent heat fluxes in most models (Sangelantoni et al. submitted). This explains the higher temperatures as well as the lack of moisture in the boundary layer making the deficit to saturation more difficult to sustain. The moistening of the lower free troposphere is then more difficult and conditional instability that yields the onset of convection occurs at higher values of IWV. In contrast to the land, over the sea, precipitation triggering depends on large scale convergence which is the main process allowing lifting of the particles, but the saturation deficit increases with temperature and becomes much more difficult to break through in the higher temperature bins. This effect is increased in the ensemble with explicit convection, while surface humidity is not a limiting factor. Additional information about vertical structure of humidity and temperature would help in the understanding of these differences, in particular to differentiate between the impacts of the boundary layer and lower free-troposphere.

In this study, the impact of convection representation (explicit versus parameterized) cannot be assessed fully because of the lack of simulations without convective schemes at 0.11° resolution. For the first time and very recently, an ensemble of climate simulations using explicit convection at 0.11° has been performed and the analysis of these simulations will help to disentangle what comes from the resolution and what comes from the convection representation.

Finally, the daily time scale is considered because of the availability of data in EURO- and Med-CORDEX ensembles. This is not the best time scale for addressing the rapid processes in convective events, which often occur over much shorter periods (Schiro et al. 2016). The next step will be to assess the processes of triggering at hourly time scales and to use an ensemble of climate projections to investigate the evolution of these convective transition processes and of precipitation distribution in a warming climate.

**Acknowledgements** All authors gratefully acknowledge the WCRP-CORDEX-FPS on Convective phenomena at high resolution over Europe and the Mediterranean (FPSCONVALP- 3) and the research data exchange infrastructure and services provided by the Jülich

Supercomputing Centre, Germany, as part of the Helmholtz Data Federation initiative. To process the data, this study benefited from the IPSL mesocenter ESPRI facility which is supported by CNRS, UPMC, Labex L-IPSL, CNES and Ecole Polytechnique, and received funding from the HORIZON 2020 EUCP (European Climate Prediction System) project (<https://www.eucp-project.eu>, grant agreement No. 776613). IPSL, CNRM and SMHI also acknowledge funding from the HORIZON 2020 EUCP. IPSL's simulation was granted access to the HPC resources of IDRIS under the allocations of the project 0227 "Fonctionnement de la Mediterranee : circulation et ecosystemes" and HPC resources of TGCC under the allocation A0090106877 made by GENCI. The GPS and SIRTAReOBS datasets are maintained by the French national center for Atmospheric data and services AERIS and Research Infrastructure ACTRIS-FR. J.M. acknowledges the support of the Spanish Government through the Agencia Estatal de Investigación (project PID2019-111481RB-I00 and "Unidad de excelencia María de Maeztu" MdM-2017-0765). Ø.H. has received support from the project GREAT, funded by the Research Council of Norway (grant no. 275589), and acknowledge computing resources from Notur (NN9188K). AUTH simulations were supported by computational time granted from the National Infrastructures for Research and Technology S.A. (GRNET S.A.) in the National HPC facility—ARIS—under project pr009020\_thin. UCAN simulations have been carried out on the Altamira Supercomputer at the Instituto de Física de Cantabria (IFCA-CSIC), member of the Spanish Supercomputing Network. JF acknowledges support from project CORDyS (PID2020-116595RB-I00) funded by MCIN/AEI/10.13039/501100011033. K.G. and H.T. acknowledge the computing time granted by the John von Neumann Institute for Computing (NIC) and through JARA-HPC on the supercomputer JURECA at the Jülich Supercomputing Centre (JSC) through the grant JJSC39. H.T. additionally acknowledges the support received via the project "reclip:convex", funded by the Austrian Climate Research Programme (ACRP) of the Klima- und Energiefonds (no. B769999), the Vienna Scientific Cluster (VSC) via the grants 70992 and 71193, as well as the cooperation project GEOCLIM Data Infrastructure Austria, funded by the Austrian Education, Science and Research Ministry (BMBWF).

**Author contributions** The analysis has been performed by Ha T-M, Bastin S. and Drobinski P. and other co-authors provided the datasets. All authors have read the paper and gave feedbacks to improve the paper and agreed to the published version of the manuscript.

**Data availability** Output from EURO-CORDEX simulations are available at <https://esgf-node.ipsl.upmc.fr/search/cordex-ipsl>; Output from Med-CORDEX simulations are available at <https://www.medcordex.eu/search/index.php>; FPSCONV simulations during the current study are not publicly available but are available from the co-authors on reasonable request; ERA5 tropospheric temperature is available at <https://www.ecmwf.int/en/forecasts/datasets/reanalysis-datasets/era5>; SIRTAReOBS, GNSS IWV and gridded precipitation are provided by co-authors.

## Declarations

**Conflicts of interests** The authors declare that they have no conflict of interest.

**Open Access** This article is licensed under a Creative Commons Attribution 4.0 International License, which permits use, sharing, adaptation, distribution and reproduction in any medium or format, as long as you give appropriate credit to the original author(s) and the source, provide a link to the Creative Commons licence, and indicate if changes were made. The images or other third party material in this article are included in the article's Creative Commons licence, unless indicated

otherwise in a credit line to the material. If material is not included in the article's Creative Commons licence and your intended use is not permitted by statutory regulation or exceeds the permitted use, you will need to obtain permission directly from the copyright holder. To view a copy of this licence, visit <http://creativecommons.org/licenses/by/4.0/>.

## References

- Adinolfi M, Raffa M, Reder A, Mercogliano P (2020) Evaluation and expected changes of summer precipitation at convection permitting Scale with COSMO-CLM over alpine space. *Atmosphere* 12:54. <https://doi.org/10.3390/atmos12010054>
- Ahrens B, Meier T, Brisson E (2020) Diurnal Cycle of Precipitation in the Himalayan Foothills – Observations and Model Results. In: Dimri AP, Bookhagen B, Stoffel M, Yasunari T (eds) *Himalayan Weather and Climate and their Impact on the Environment*. Springer International Publishing, Cham, pp 73–89
- Argüeso D, Romero R, Homar V (2020) Precipitation Features of the Maritime Continent in Parameterized and Explicit Convection Models. *J Clim* 33:2449–2466. <https://doi.org/10.1175/JCLI-D-19-0416.1>
- Baldauf M, Seifert A, Förstner J et al (2011) Operational Convective-Scale Numerical Weather Prediction with the COSMO Model: Description and Sensitivities. *Mon Weather Rev* 139:3887–3905. <https://doi.org/10.1175/MWR-D-10-05013.1>
- Ban N, Schmidli J, Schär C (2014) Evaluation of the convection-resolving regional climate modeling approach in decade-long simulations. *J Geophys Res Atmos* 119:7889–7907. <https://doi.org/10.1002/2014JD021478>
- Ban N, Caillaud C, Coppola E et al (2021) The first multi-model ensemble of regional climate simulations at kilometer-scale resolution, part I: evaluation of precipitation. *Clim Dyn* 57:275–302. <https://doi.org/10.1007/s00382-021-05708-w>
- Bastin S, Drobinski P (2006) Sea-breeze-induced mass transport over complex terrain in south-eastern France: A case-study. *Q J R Meteorol Soc* 132:405–423. <https://doi.org/10.1256/qj.04.111>
- Bastin S, Chiriac M, Drobinski P (2018) Control of radiation and evaporation on temperature variability in a WRF regional climate simulation: comparison with colocated long term ground based observations near Paris. *Clim Dyn* 51:985–1003. <https://doi.org/10.1007/s00382-016-2974-1>
- Bastin S, Drobinski P, Chiriac M et al (2019) Impact of humidity biases on light precipitation occurrence: observations versus simulations. *Atmos Chem Phys* 19:1471–1490. <https://doi.org/10.5194/acp-19-1471-2019>
- Bauer H-S, Weusthoff T, Dorninger M et al (2011) Predictive skill of a subset of models participating in D-PHASE in the COPS region: Predictive Skill of a Subset of D-PHASE Models. *QJR Meteorol Soc* 137:287–305. <https://doi.org/10.1002/qj.715>
- Belušić D, de Vries H, Dobler A et al (2020) HCLIM38: a flexible regional climate model applicable for different climate zones from coarse to convection-permitting scales. *Geosci Model Dev* 13:1311–1333. <https://doi.org/10.5194/gmd-13-1311-2020>
- Berthou S, Rowell DP, Kendon EJ et al (2019) Improved climatological precipitation characteristics over West Africa at convection-permitting scales. *Clim Dyn* 53:1991–2011. <https://doi.org/10.1007/s00382-019-04759-4>
- Berthou S, Kendon EJ, Chan SC et al (2020) Pan-European climate at convection-permitting scale: a model intercomparison study. *Clim Dyn* 55:35–59. <https://doi.org/10.1007/s00382-018-4114-6>
- Boberg F, Berg P, Thejll P et al (2009) Improved confidence in climate change projections of precipitation evaluated using daily

- statistics from the PRUDENCE ensemble. *Clim Dyn* 32:1097–1106. <https://doi.org/10.1007/s00382-008-0446-y>
- Bock O, (2021) GNSS Integrated Water Vapour data over France and Europe, for EURO- and Med-CORDEX. *Aeris*. <https://doi.org/10.25326/294>
- Brockhaus P, Lüthi D, Schär C (2008) Aspects of the diurnal cycle in a regional climate model. *metz* 17:433–443. <https://doi.org/10.1127/0941-2948/2008/0316>
- Brown JR, Jakob C, Haynes JM (2010) An Evaluation of Rainfall Frequency and Intensity over the Australian Region in a Global Climate Model. *J Clim* 23:6504–6525. <https://doi.org/10.1175/2010JCLI3571.1>
- Caillaud C, Somot S, Alias A et al (2021) Modelling Mediterranean heavy precipitation events at climate scale: an object-oriented evaluation of the CNRM-AROME convection-permitting regional climate model. *Clim Dyn* 56:1717–1752. <https://doi.org/10.1007/s00382-020-05558-y>
- Cattiaux J, Vautard R, Cassou C, et al (2010) Winter 2010 in Europe: A cold extreme in a warming climate: COLD WINTER 2010 IN EUROPE. *Geophys Res Lett* 37:n/a-n/a. <https://doi.org/10.1029/2010GL044613>
- Chiriaco M, Bastin S, Yiou P et al (2014) European heatwave in July 2006: Observations and modeling showing how local processes amplify conducive large-scale conditions: July 2006 heatwave at SIRTA observatory. *Geophys Res Lett* 41:5644–5652. <https://doi.org/10.1002/2014GL060205>
- Chiriaco M, Dupont J-C, Bastin S et al (2018) ReOBS: a new approach to synthesize long-term multi-variable dataset and application to the SIRTA supersite. *Earth Syst Sci Data* 10:919–940. <https://doi.org/10.5194/essd-10-919-2018>
- Coppola E, Sobolowski S, Pichelli E et al (2020) A first-of-its-kind multi-model convection permitting ensemble for investigating convective phenomena over Europe and the Mediterranean. *Clim Dyn* 55:3–34. <https://doi.org/10.1007/s00382-018-4521-8>
- Corti S, Molteni F, Palmer TN (1999) Signature of recent climate change in frequencies of natural atmospheric circulation regimes. *Nature* 398:799–802. <https://doi.org/10.1038/19745>
- Dai A (2006) Precipitation Characteristics in Eighteen Coupled Climate Models. *J Clim* 19:4605–4630. <https://doi.org/10.1175/JCLI3884.1>
- Dai A, Trenberth KE (2004) The Diurnal Cycle and Its Depiction in the Community Climate System Model. *J Climate* 17:930–951. [https://doi.org/10.1175/1520-0442\(2004\)017%3c0930:TDCAID%3e2.0.CO;2](https://doi.org/10.1175/1520-0442(2004)017%3c0930:TDCAID%3e2.0.CO;2)
- Feser F, von Storch H (2005) A Spatial Two-Dimensional Discrete Filter for Limited-Area-Model Evaluation Purposes. *Mon Weather Rev* 133:1774–1786. <https://doi.org/10.1175/MWR2939.1>
- Flaounas E, Davolio S, Raveh-Rubin S et al (2022) Mediterranean cyclones: current knowledge and open questions on dynamics, prediction, climatology and impacts. *Weather Clim Dynam* 3:173–208. <https://doi.org/10.5194/wcd-3-173-2022>
- Foley AM (2010) Uncertainty in regional climate modelling: A review. *Progress in Physical Geography: Earth and Environment* 34:647–670. <https://doi.org/10.1177/0309133310375654>
- Fosser G, Khodayar S, Berg P (2015) Benefit of convection permitting climate model simulations in the representation of convective precipitation. *Clim Dyn* 44:45–60. <https://doi.org/10.1007/s00382-014-2242-1>
- Froidevaux P, Schlemmer L, Schmidli J et al (2014) Influence of the Background Wind on the Local Soil Moisture-Precipitation Feedback. *J Atmos Sci* 71:782–799. <https://doi.org/10.1175/JAS-D-13-0180.1>
- Fumière Q, Déqué M, Nuissier O et al (2020) Extreme rainfall in Mediterranean France during the fall: added value of the CNRM-AROME Convection-Permitting Regional Climate Model. *Clim Dyn* 55:77–91. <https://doi.org/10.1007/s00382-019-04898-8>
- Giorgi F, Torma C, Coppola E et al (2016) Enhanced summer convective rainfall at Alpine high elevations in response to climate warming. *Nature Geosci* 9:584–589. <https://doi.org/10.1038/ngeo2761>
- Giorgi F (2019) Thirty Years of Regional Climate Modeling: Where Are We and Where Are We Going next? *J Geophys Res Atmos* 2018JD030094. <https://doi.org/10.1029/2018JD030094>
- Guo Z, Fang J, Sun X et al (2019) Sensitivity of Summer Precipitation Simulation to Microphysics Parameterization Over Eastern China: Convection-Permitting Regional Climate Simulation. *J Geophys Res Atmos* 124:9183–9204. <https://doi.org/10.1029/2019JD030295>
- Guo Z, Fang J, Sun X et al (2020) Decadal long convection-permitting regional climate simulations over eastern China: evaluation of diurnal cycle of precipitation. *Clim Dyn* 54:1329–1349. <https://doi.org/10.1007/s00382-019-05061-z>
- Haefelin M, Barthès L, Bock O et al (2005) SIRTA, a ground-based atmospheric observatory for cloud and aerosol research. *Ann Geophys* 23:253–275. <https://doi.org/10.5194/angeo-23-253-2005>
- Hersbach H, Bell W, Berrisford P, et al (2019) Global reanalysis: goodbye ERA-Interim, hello ERA5. <https://doi.org/10.21957/VF291HEHD7>
- Hodnebrog Ø, Marelle L, Alterskjær K et al (2019) Intensification of summer precipitation with shorter time-scales in Europe. *Environ Res Lett* 14:124050. <https://doi.org/10.1088/1748-9326/ab549c>
- Hohenegger C, Brockhaus P, Bretherton CS, Schär C (2009) The Soil Moisture-Precipitation Feedback in Simulations with Explicit and Parameterized Convection. *J Clim* 22:5003–5020. <https://doi.org/10.1175/2009JCLI2604.1>
- Hohenegger C, Brockhaus P, Schär C (2008) Towards climate simulations at cloud-resolving scales. *metz* 17:383–394. <https://doi.org/10.1127/0941-2948/2008/0303>
- Holloway CE, Neelin JD (2009) Moisture Vertical Structure, Column Water Vapor, and Tropical Deep Convection. *J Atmos Sci* 66:1665–1683. <https://doi.org/10.1175/2008JAS2806.1>
- IPCC, 2021: Climate Change 2021: The Physical Science Basis. Contribution of Working Group I to the Sixth Assessment Report of the Intergovernmental Panel on Climate Change [Masson-Delmotte, V., P. Zhai, A. Pirani, S.L. Connors, C. Péan, S. Berger, N. Caud, Y. Chen, L. Goldfarb, M.I. Gomis, M. Huang, K. Leitzell, E. Lonnoy, J.B.R. Matthews, T.K. Maycock, T. Waterfield, O. Yelekçi, R. Yu, and B. Zhou (eds.)]. Cambridge University Press. Cambridge University Press, Cambridge, United Kingdom and New York, NY, USA, In press, doi:<https://doi.org/10.1017/9781009157896>.
- Isotta FA, Frei C, Weigluni V et al (2014) The climate of daily precipitation in the Alps: development and analysis of a high-resolution grid dataset from pan-Alpine rain-gauge data: CLIMATE OF DAILY PRECIPITATION IN THE ALPS. *Int J Climatol* 34:1657–1675. <https://doi.org/10.1002/joc.3794>
- Jacob D, Petersen J, Eggert B et al (2014) EURO-CORDEX: new high-resolution climate change projections for European impact research. *Reg Environ Change* 14:563–578. <https://doi.org/10.1007/s10113-013-0499-2>
- Keller M, Fuhrer O, Schmidli J, et al (2016) Evaluation of convection-resolving models using satellite data: The diurnal cycle of summer convection over the Alps. *metz* 25:165–179. <https://doi.org/10.1127/metz/2015/0715>
- Kendon EJ, Roberts NM, Senior CA, Roberts MJ (2012) Realism of Rainfall in a Very High-Resolution Regional Climate Model. *J Clim* 25:5791–5806. <https://doi.org/10.1175/JCLI-D-11-00562.1>
- Kendon EJ, Roberts NM, Fowler HJ et al (2014) Heavier summer downpours with climate change revealed by weather forecast resolution model. *Nature Clim Change* 4:570–576. <https://doi.org/10.1038/nclimate2258>




- Kendon EJ, Ban N, Roberts NM et al (2017) Do Convection-Permitting Regional Climate Models Improve Projections of Future Precipitation Change? *Bull Am Meteor Soc* 98:79–93. <https://doi.org/10.1175/BAMS-D-15-0004.1>
- Kendon EJ, Stratton RA, Tucker S et al (2019) Enhanced future changes in wet and dry extremes over Africa at convection-permitting scale. *Nat Commun* 10:1794. <https://doi.org/10.1038/s41467-019-09776-9>
- Kjellström E, Boberg F, Castro M et al (2010) Daily and monthly temperature and precipitation statistics as performance indicators for regional climate models. *Clim Res* 44:135–150. <https://doi.org/10.3354/cr00932>
- Knist S, Goergen K, Simmer C (2020) Effects of land surface inhomogeneity on convection-permitting WRF simulations over central Europe. *Meteorol Atmos Phys* 132:53–69. <https://doi.org/10.1007/s00703-019-00671-y>
- Konduru RT, Takahashi HG (2020) Effects of Convection Representation and Model Resolution on Diurnal Precipitation Cycle Over the Indian Monsoon Region: Toward a Convection-Permitting Regional Climate Simulation. *J Geophys Res Atmos*. <https://doi.org/10.1029/2019JD032150>
- Kouadio K, Bastin S, Konare A, Ajayi VO (2020) Does convection-permitting simulate better rainfall distribution and extreme over Guinean coast and surroundings? *Clim Dyn* 55:153–174. <https://doi.org/10.1007/s00382-018-4308-y>
- Kuo Y-H, Neelin JD, Mechoso CR (2017) Tropical Convective Transition Statistics and Causality in the Water Vapor-Precipitation Relation. *J Atmos Sci* 74:915–931. <https://doi.org/10.1175/JAS-D-16-0182.1>
- Langhans W, Schmidli J, Fuhrer O et al (2013) Long-Term Simulations of Thermally Driven Flows and Orographic Convection at Convection-Parameterizing and Cloud-Resolving Resolutions. *J Appl Meteorol Climatol* 52:1490–1510. <https://doi.org/10.1175/JAMC-D-12-0167.1>
- Lavin-Gullon A, Fernandez J, Bastin S et al (2021) Internal variability versus multi-physics uncertainty in a regional climate model. *Int J Climatol*. <https://doi.org/10.1002/joc.6717>
- Lenderink G, van Meijgaard E (2008) Increase in hourly precipitation extremes beyond expectations from temperature changes. *Nature Geosci* 1:511–514. <https://doi.org/10.1038/ngeo262>
- Leutwyler D, Lüthi D, Ban N et al (2017) Evaluation of the convection-resolving climate modeling approach on continental scales: CONVECTION-RESOLVING CONTINENTAL-SCALE SIMULATION. *J Geophys Res Atmos* 122:5237–5258. <https://doi.org/10.1002/2016JD026013>
- Lind P, Lindstedt D, Kjellström E, Jones C (2016) Spatial and Temporal Characteristics of Summer Precipitation over Central Europe in a Suite of High-Resolution Climate Models. *J Clim* 29:3501–3518. <https://doi.org/10.1175/JCLI-D-15-0463.1>
- Liu C, Ikeda K, Rasmussen R et al (2017) Continental-scale convection-permitting modeling of the current and future climate of North America. *Clim Dyn* 49:71–95. <https://doi.org/10.1007/s00382-016-3327-9>
- Lucas C, Zipser EJ, Lemone MA (1994) Vertical Velocity in Oceanic Convection off Tropical Australia. *J Atmos Sci* 51:3183–3193. [https://doi.org/10.1175/1520-0469\(1994\)051%3c3183:VVI-OCO%3e2.0.CO;2](https://doi.org/10.1175/1520-0469(1994)051%3c3183:VVI-OCO%3e2.0.CO;2)
- Lucas-Picher P, Argüeso D, Brisson E et al (2021) Convection-permitting modeling with regional climate models: Latest developments and next steps. *Wires Clim Change*. <https://doi.org/10.1002/wcc.731>
- Lundquist J, Hughes M, Gutmann E, Kapnick S (2019) Our Skill in Modeling Mountain Rain and Snow is Bypassing the Skill of Our Observational Networks. *Bull Am Meteor Soc* 100:2473–2490. <https://doi.org/10.1175/BAMS-D-19-0001.1>
- Lüthi S, Ban N, Kotlarski S et al (2019) Projections of Alpine Snow-Cover in a High-Resolution Climate Simulation. *Atmosphere* 10:463. <https://doi.org/10.3390/atmos10080463>
- Nabat P, Somot S, Cassou C et al (2020) Modulation of radiative aerosols effects by atmospheric circulation over the Euro-Mediterranean region. *Atmos Chem Phys* 20:8315–8349. <https://doi.org/10.5194/acp-20-8315-2020>
- Neelin JD, Peters O, Hales K (2009) The Transition to Strong Convection. *J Atmos Sci* 66:2367–2384. <https://doi.org/10.1175/2009JAS2962.1>
- Ning T, Elgered G, Willén U, Johansson JM (2013) Evaluation of the atmospheric water vapor content in a regional climate model using ground-based GPS measurements: EVALUATION OF CLIMATE MODELS USING GPS. *J Geophys Res Atmos* 118:329–339. <https://doi.org/10.1029/2012JD018053>
- Nuissier O, Joly B, Joly A et al (2011) A statistical downscaling to identify the large-scale circulation patterns associated with heavy precipitation events over southern France: Synoptic-Scale Ingredients for Heavy Precipitation Events. *QJR Meteorol Soc* 137:1812–1827. <https://doi.org/10.1002/qj.866>
- Piazza M, Prein AF, Truhetz H, Csaki A (2019) On the sensitivity of precipitation in convection-permitting climate simulations in the Eastern Alpine region. *metz* 28:323–346. <https://doi.org/10.1127/metz/2019/0941>
- Prein AF, Gobiet A, Suklitsch M et al (2013) Added value of convection-permitting seasonal simulations. *Clim Dyn* 41:2655–2677. <https://doi.org/10.1007/s00382-013-1744-6>
- Prein AF, Langhans W, Fosser G et al (2015) A review on regional convection-permitting climate modeling: Demonstrations, prospects, and challenges. *Rev Geophys* 53:323–361. <https://doi.org/10.1002/2014RG000475>
- Quintana-Seguí P, Le Moigne P, Durand Y et al (2008) Analysis of Near-Surface Atmospheric Variables. *J Appl Meteorol Climatol* 47:92–107
- Rasmussen R, Liu C, Ikeda K et al (2011) High-Resolution Coupled Climate Runoff Simulations of Seasonal Snowfall over Colorado: A Process Study of Current and Warmer Climate. *J Clim* 24:3015–3048. <https://doi.org/10.1175/2010JCLI3985.1>
- Rasmussen R, Ikeda K, Liu C et al (2014) Climate Change Impacts on the Water Balance of the Colorado Headwaters. *J Hydrometeorol* 15:1091–1116
- Rasmussen KL, Prein AF, Rasmussen RM et al (2020) Changes in the convective population and thermodynamic environments in convection-permitting regional climate simulations over the United States. *Clim Dyn* 55:383–408. <https://doi.org/10.1007/s00382-017-4000-7>
- Rauthe M, Steiner H, Riediger U et al (2013) A Central European precipitation climatology ? Part I: Generation and validation of a high-resolution gridded daily data set (HYRAS). *Meteorol Z* 22:235–256. <https://doi.org/10.1127/0941-2948/2013/0436>
- Reder A, Raffa M, Montesarchio M, Mercogliano P (2020) Performance evaluation of regional climate model simulations at different spatial and temporal scales over the complex orography area of the Alpine region. *Nat Hazards* 102:151–177. <https://doi.org/10.1007/s11069-020-03916-x>
- Rockel B, Will A, Hense A (2008) The Regional Climate Model COSMO-CLM (CCLM). *metz* 17:347–348. <https://doi.org/10.1127/0941-2948/2008/0309>
- Ruti PM, Somot S, Giorgi F et al (2016) Med-CORDEX Initiative for Mediterranean Climate Studies. *Bull Am Meteor Soc* 97:1187–1208. <https://doi.org/10.1175/BAMS-D-14-00176.1>
- Sahany S, Neelin JD, Hales K, Neale RB (2012) Temperature-Moisture Dependence of the Deep Convective Transition as a Constraint on Entrainment in Climate Models. *J Atmos Sci* 69:1340–1358. <https://doi.org/10.1175/JAS-D-11-0164.1>

- Sahany S, Neelin JD, Hales K, Neale RB (2014) Deep Convective Transition Characteristics in the Community Climate System Model and Changes under Global Warming. *J Clim* 27:9214–9232. <https://doi.org/10.1175/JCLI-D-13-00747.1>
- Schiro KA, Neelin JD, Adams DK, Lintner BR (2016) Deep Convection and Column Water Vapor over Tropical Land versus Tropical Ocean: A Comparison between the Amazon and the Tropical Western Pacific. *J Atmos Sci* 73:4043–4063. <https://doi.org/10.1175/JAS-D-16-01119.1>
- Seager R, Hooks A, Williams AP et al (2015) Climatology, Variability, and Trends in the U.S. Vapor Pressure Deficit, an Important Fire-Related Meteorological Quantity. *J Appl Meteorol Climatol* 54:1121–1141. <https://doi.org/10.1175/JAMC-D-14-0321.1>
- Seager R, Liu H, Kushnir Y et al (2020) Mechanisms of Winter Precipitation Variability in the European-Mediterranean Region Associated with the North Atlantic Oscillation. *J Clim* 33:7179–7196. <https://doi.org/10.1175/JCLI-D-20-0011.1>
- Skamarock W, Klemp J, Dudhia J, et al (2008) A Description of the Advanced Research WRF Version 3. UCAR/NCAR
- Stephens GL, L'Ecuyer T, Forbes R et al (2010) Dreary state of precipitation in global models: MODEL AND OBSERVED PRECIPITATION. *J Geophys Res*. <https://doi.org/10.1029/2010JD014532>
- Sun Y, Solomon S, Dai A, Portmann RW (2006) How Often Does It Rain? *J Clim* 19:916–934. <https://doi.org/10.1175/JCLI3672.1>
- Tompkins AM (2001) Organization of Tropical Convection in Low Vertical Wind Shears: The Role of Water Vapor. *J Atmos Sci* 58:529–545. [https://doi.org/10.1175/1520-0469\(2001\)058%3c0529:OOTCIL%3e2.0.CO;2](https://doi.org/10.1175/1520-0469(2001)058%3c0529:OOTCIL%3e2.0.CO;2)
- Trigo R, Xoplaki E, Zorita E, et al (2006) Relations between Variability in the Mediterranean Region and Mid-Latitude Variability. In: *Mediterranean Climate Variability*. pp 179–226
- Vidal J-P, Martin E, Franchistéguy L et al (2010) A 50-year high-resolution atmospheric reanalysis over France with the Safran system: A 50-YEAR HIGH-RESOLUTION ATMOSPHERIC REANALYSIS OVER FRANCE. *Int J Climatol* 30:1627–1644. <https://doi.org/10.1002/joc.2003>
- Weisman ML, Skamarock WC, Klemp JB (1997) The Resolution Dependence of Explicitly Modeled Convective Systems. *Mon Wea Rev* 125:527–548. [https://doi.org/10.1175/1520-0493\(1997\)125%3c0527:TRDOEM%3e2.0.CO;2](https://doi.org/10.1175/1520-0493(1997)125%3c0527:TRDOEM%3e2.0.CO;2)
- Winterfeldt J, Weisse R (2009) Assessment of Value Added for Surface Marine Wind Speed Obtained from Two Regional Climate Models. *Mon Weather Rev* 137:2955–2965. <https://doi.org/10.1175/2009MWR2704.1>
- Wulfmeyer V, Muppa SK, Behrendt A et al (2016) Determination of Convective Boundary Layer Entrainment Fluxes, Dissipation Rates, and the Molecular Destruction of Variances: Theoretical Description and a Strategy for Its Confirmation with a Novel Lidar System Synergy. *J Atmos Sci* 73:667–692. <https://doi.org/10.1175/JAS-D-14-0392.1>
- Xoplaki E, González-Rouco JF, Luterbacher J, Wanner H (2003) Mediterranean summer air temperature variability and its connection to the large-scale atmospheric circulation and SSTs. *Clim Dyn* 20:723–739. <https://doi.org/10.1007/s00382-003-0304-x>
- Yiou P, Goubanova K, Li ZX, Nogaj M (2008) Weather regime dependence of extreme value statistics for summer temperature and precipitation. *Nonlin Processes Geophys* 15:365–378. <https://doi.org/10.5194/npg-15-365-2008>
- Yiou P, Nogaj M (2004) Extreme climatic events and weather regimes over the North Atlantic: When and where?: WEATHER REGIMES AND EXTREMES. *Geophys Res Lett* 31:n/a-n/a. <https://doi.org/10.1029/2003GL019119>
- Zeman C, Wedi NP, Dueben PD et al (2021) Model intercomparison of COSMO 5.0 and IFS 45r1 at kilometer-scale grid spacing. *Geosci Model Dev* 14:4617–4639. <https://doi.org/10.5194/gmd-14-4617-2021>

**Publisher's Note** Springer Nature remains neutral with regard to jurisdictional claims in published maps and institutional affiliations.

## Authors and Affiliations

Minh T. Ha<sup>1</sup>  · Sophie Bastin<sup>1</sup> · Philippe Drobinski<sup>2</sup> · L. Fita<sup>3</sup> · J. Polcher<sup>2</sup> · O. Bock<sup>4,5</sup> · M. Chiriaco<sup>1</sup> · D. Belušić<sup>6,17</sup> · C. Caillaud<sup>7</sup> · A. Dobler<sup>8</sup> · J. Fernandez<sup>9</sup> · K. Goergen<sup>10</sup> · Ø. Hodnebrog<sup>11</sup> · S. Kartsios<sup>12</sup> · E. Katragkou<sup>12</sup> · A. Lavin-Gullon<sup>9</sup> · T. Lorenz<sup>13</sup> · J. Milovac<sup>9</sup> · H.-J. Panitz<sup>14</sup> · S. Sobolowski<sup>13</sup> · H. Truhetz<sup>15</sup> · K. Warrach-Sagi<sup>16</sup> · V. Wulfmeyer<sup>16</sup>

<sup>1</sup> Laboratoire ATmosphere Milieux Observations Spatiales (LATMOS)/Institut Pierre Simon Laplace (IPSL), Sorbonne Université, UVSQ Université Paris-Saclay, CNRS, ParisGuyancourt, France

<sup>2</sup> Laboratoire de Météorologie Dynamique (LMD)/IPSL, Ecole Polytechnique, CNRS, Palaiseau, France

<sup>3</sup> Centro de Investigaciones del Mar y la Atmósfera (CIMA), CONICET-UBA, CNRS IRL-IFAECI, Buenos Aires, Argentina

<sup>4</sup> Université de Paris, Institut de Physique du Globe de Paris, CNRS, 75005 Paris, IGN, France

<sup>5</sup> ENSG-Géomatique, IGN, 77455 Marne-la-Vallée, France

<sup>6</sup> Swedish Meteorological and Hydrological Institute (SMHI), Norrköping, Sweden

<sup>7</sup> CNRM, CNRS Université Paul Sabatier, Météo-France, Toulouse, France

<sup>8</sup> Norwegian Meteorological Institute, Henrik Mohns Plass 1, 0313 Oslo, Norway

<sup>9</sup> Meteorology Group, Instituto de Física de Cantabria (IFCA), CSIC-Univ. Cantabria, Santander, Spain

<sup>10</sup> Institute of Bio- and Geosciences (IBG-3, Agrosphere), Research Centre Jülich, Jülich, Germany

<sup>11</sup> Center for International Climate Research (CICERO), Oslo, Norway

<sup>12</sup> Department of Meteorology and Climatology, School of Geology, Aristotle University of Thessaloniki, Thessaloniki, Greece

<sup>13</sup> NORCE Norwegian Research Centre, Bjerknes Centre for Climate Research, Bergen, Norway

- <sup>14</sup> Institute of Meteorology and Climate Research, Karlsruhe Institute of Technology (KIT), IMK-TRO, Karlsruhe, Germany
- <sup>15</sup> Wegener Center for Climate and Global Change (WEGC), University of Graz, Graz, Austria

- <sup>16</sup> Institute of Physics and Meteorology, University of Hohenheim, Stuttgart, Germany
- <sup>17</sup> Department of Geophysics, Faculty of Science, University of Zagreb, Zagreb, Croatia